

45 point is controlled by both stratospheric and tropospheric processes. Residual variability of the
46 cold point temperature not captured by the MLR is still connected to temperature variability in
47 the stratosphere.

48

49 **1 Introduction**

50 The tropical tropopause layer (TTL) is a transition layer between the tropical troposphere
51 and stratosphere and extends from the level of zero net radiative heating to the maximum height
52 where clouds still exist (~14.5 to ~18.5 km) (e.g., Gettelman et al., 2004; Fu et al., 2007;
53 Fueglistaler et al., 2009). A crucial component of the TTL is the water vapor and ice that exists
54 there. Water vapor in the TTL can transit into the stratosphere, where it has significant impacts
55 on Earth's radiation budget and stratospheric ozone (Mote et al., 1996; Forster and Shine, 1999;
56 Kirk-Davidoff et al., 1999; Fueglistaler and Haynes, 2005; Solomon et al., 2010; Joshi et al.,
57 2010; Flury et al., 2012; Ding & Fu, 2018; Randel and Park, 2019). Ice in this region exists as
58 thin and extensive cirrus referred to as TTL cirrus clouds. These clouds can impact the TTL's
59 local radiative heating rate, which may influence the upwelling and temperatures in the TTL
60 (McFarquhar et al., 2000; Corti et al., 2006; Yang et al., 2010; Dinh et al., 2010; Fu et al., 2018;
61 Wang and Fu, 2021). These cirrus clouds might also contribute a warming effect on the surface
62 (Zhou et al., 2014). Despite their importance, climate models have difficulty simulating
63 stratospheric water vapor concentrations and TTL cirrus clouds (Gettelman et al., 2009;
64 Gettelman et al., 2010; Randel and Jensen, 2013; Hardiman et al., 2015; Wang and Fu, 2021).

65 The water vapor going into the stratosphere is largely regulated by the coldest
66 temperatures that air experiences in the TTL, especially during boreal winter (Holton and
67 Gettelman, 2001). Cold temperature anomalies in the TTL can largely limit the entry of water
68 vapor into the stratosphere through the formation of TTL cirrus clouds (Jensen, 1996; Flury et
69 al., 2012; Jensen et al., 2013; Randel and Jensen, 2013). Temperature variability in this region is
70 a result of both stratospheric and tropospheric modes of large-scale variability (Randel and Wu,
71 2015; Charlesworth et al., 2019; Lu et al., 2020). Observed interannual variations in TTL
72 temperature, water vapor, and clouds have been linked to stratospheric modes including the
73 Quasi-Biennial Oscillation (QBO) and Brewer Dobson circulation (BDC) and tropospheric
74 modes including the El Niño Southern Oscillation (ENSO) and Madden-Julian Oscillation
75 (MJO) (Virts and Wallace, 2010; Eguchi and Kodera, 2010; Liang et al., 2011; Davis et al.,
76 2013; Li and Thompson, 2013; Virts and Wallace, 2014; Ding and Fu, 2018; Tseng and Fu,
77 2017a; Tseng and Fu, 2017b; Ye et al., 2018; Sweeney et al., 2023). Wave activity on a variety
78 of temporal and spatial scales can also impact TTL temperatures and cirrus clouds based on both
79 observational and modeling studies (Boehm and Verlinde, 2000; Grise and Thompson, 2013;
80 Kim and Alexander, 2015; Podglajen et al., 2016; Kim et al., 2016; Podglajen et al., 2018; Chang
81 and L'Ecuyer, 2020; Bramberger et al., 2022).

82 An open question remains to what extent these observed interannual variations are
83 governed by stratospheric versus tropospheric processes (Garfinkel et al., 2013; Fu, 2013; Ding
84 and Fu, 2018). This question is important because the decadal TTL variability has been linked to
85 both (Solomon et al., 2010; Garfinkel et al., 2013; Xie et al., 2014; Lu et al., 2020). Despite the
86 different sources of the variability, their influence on the TTL variability may involve common
87 mechanisms by e.g., modulation of the TTL upwelling, complicating the partitioning of the
88 sources (Austin and Reicher, 2008; Lin et al., 2017). This question is also important because
89 connections between TTL variables and the modes of large-scale variability found in
90 observations may help validate models' representation of the TTL. This study attempts to shed

91 light on this question by examining key target variables in the TTL like temperature, water
92 vapor, ozone, and cloud fraction observed from radio occultations, the Microwave Limb Sounder
93 aboard the Aura satellite, and the CALIOP instrument. The explained variance of these target
94 variables is investigated by employing a multiple linear regression (MLR) where predictors are
95 the QBO, BDC, T500, and MJO (Dessler et al., 2013; Dessler et al., 2014; Tseng and Fu, 2017a;
96 Wang et al., 2019).

97 98 **2 Data**

99 **2.1 Target Variables**

100 2.1.1 Temperature

101 Temperature data come from Radio Occultation (RO) profiles from the COSMIC-1 and 2
102 as well as the MetOp-A, B, and C satellites, archived at the University Corporation for
103 Atmospheric Research (Anthes et al., 2008; Schreiner et al., 2020). Data was preprocessed using
104 the level 2 WetPrf product from June 2006 to December of 2021 (Sweeney and Fu, 2021). These
105 RO temperature profiles have high accuracy (less than 0.1 K). RO data have high vertical
106 resolution (~0.5 km) in the TTL, but coarser horizontal resolution of about 200 km (Kursinski et
107 al., 1997; Kuo et al., 2004; Zeng et al., 2019). The vertical temperature gradient and cold point
108 tropopause temperature and height are also calculated from the RO temperature data.

109 2.1.2 Clouds

110 Cloud fraction data comes from the Cloud-Aerosol Lidar with Orthogonal Polarization
111 (CALIOP) instrument aboard the CALIPSO satellite (Winker et al., 2010). CALIOP can provide
112 information of cloud layers with optical depth as small as 0.01 or less, ideal for TTL cirrus cloud
113 identification. We use the Level 2 V4.2 5-km Merged Layer Products from June of 2006 to
114 December of 2021, using only nighttime measurements to avoid solar contamination of the lidar
115 signals (Thorsen et al., 2013; Thornberry et al., 2017). Cloud fraction is derived from the lidar
116 data as the number of detections of a cloud divided by the total number of observations in each
117 2.5°x2.5° grid cell at a given level. Positive cloud identifications require Cloud-Aerosol
118 Distinction (CAD) values of greater than 30. This study uses an adapted version of the Level 2
119 V4.2 data for clouds above the lapse rate tropopause (Tseng and Fu, 2017b; Sweeney et al.,
120 2023).

121 Two different categories of clouds are identified in this study: TTL cirrus clouds which
122 are defined as clouds with bases above 14.5 km, and All clouds which are defined as clouds with
123 tops above 14.5 km irrespective of their cloud base. The 14.5 km altitude is approximately the
124 level of zero net radiative heating in the tropical atmosphere (Gettelman et al., 2004; Fu et al.,
125 2007; Tseng and Fu, 2017a). We consider TTL cirrus and All clouds separately because TTL
126 cirrus clouds are more relevant for the dehydration of the TTL, while All clouds are more
127 relevant for the total energy budget of the tropics (Corti et al., 2006; Jensen et al., 2013; Sokol
128 and Hartmann, 2020; Sweeney et al., 2023).

129 Both the TTL cirrus cloud fraction and All cloud fraction are turned into one-dimensional
130 monthly timeseries referred to as TTLCCF and ALLCF respectively. TTLCCF measures total
131 cloud fraction similarly to TTL cirrus cloud fraction described above but does not consider the
132 vertical extent of the TTL cirrus cloud (i.e., only measures whether a TTL cirrus cloud is present,
133 and not its vertical profile). ALLCF only measures whether a cloud top above 14.5 km is present,
134 and not the vertical profile of the cloud.

135 2.1.3 Water Vapor and Ozone

136 Water vapor data come from the Microwave Limb Sounder (MLS) onboard the Aura
137 Satellite (Read et al., 2007). Results regarding ozone concentrations also come from this MLS.
138 MLS measurements began in August 2004 and continue until present day. Water vapor and
139 ozone mixing ratios come from monthly mean Level 3 version 5 MLS data from June 2006 to
140 December of 2021 (Livesey et al., 2021). Tropical lower stratospheric water vapor is primarily
141 sourced from the troposphere, and transits slowly upward from the tropopause (Randel and Park.,
142 2019). Because we are particularly interested in the interannual variability of lower-stratospheric
143 water vapor, all water vapor data is lagged by one month to account for the slow transit time into
144 the lower stratosphere.

145

146 **2.2 Predictors**

147 2.2.1 Quasi-Biennial Oscillation (QBO) index

148 The QBO is the main mode of the large-scale variability in the tropical stratosphere
149 (Baldwin et al., 2001) and is a stratospheric process. The QBO index is defined using the
150 monthly mean 50 hPa zonal wind averaged over 10°S-10°N from ERA5 (Hersbach et al., 2020).
151 We let the QBO index lead the TTL variables by two months to account for the QBO
152 temperature anomaly's descent to the cold point tropopause (Dessler et al., 2013; Dessler et al.,
153 2014; Ding and Fu, 2018; Tseng and Fu, 2017a; Ye et al., 2018; Tian et al., 2019).

154 2.2.2 Madden Julian Oscillation (MJO) index

155 The MJO is the dominant mode of intraseasonal variability in the tropical atmosphere and
156 is a tropospheric process (Madden and Julian, 1971). The MJO index used here is the second
157 principal component of the velocity potential index (Ventrice et al., 2013). Maximums in this
158 MJO index are associated with peak MJO-related convection over the western Pacific and
159 suppressed convection over the eastern Indian Ocean (Virts and Wallace, 2014; Tseng and Fu,
160 2017a). We use the velocity potential index provided by the NOAA Physical Science Laboratory
161 (<https://www.psl.noaa.gov/mjo/mjoindex/>).

162 2.2.3 Temperature at 500 hPa (T500)

163 The 15°S-15°N 500 hPa temperature (T500) from the ERA5 reanalysis measures
164 tropospheric temperature. ENSO is the dominant mode of tropospheric temperature variability
165 (Philander et al., 1990). T500 is highly correlated with a three-month lead of the ENSO MEIv2
166 index ($r=0.73$) and thus implicitly captures much of the ENSO variability (Dessler et al., 2013;
167 Wang et al., 2019; Marsh and Garcia, 2007). T500 can impact the TTL through longwave
168 heating, changing tropical convective activity, and other processes (Lin et al., 2017; Ye et al.,
169 2018). Increases in T500 can dynamically induce upwelling in the TTL through the eddy
170 momentum flux convergence in the tropical upper troposphere driven by convective latent heat
171 (Boehm and Lee, 2003; Deckert and Dameris, 2008; Garny et al., 2011), which has been
172 considered part of the BDC in some studies (e.g., Boehm and Lee, 2003) but not in others (e.g.,
173 Wu and Zheng, 2022). T500 thus impacts the TTL through both thermodynamic and dynamic
174 processes and is considered a tropospheric process here.

175 2.2.4 Eddy Heat Flux Based Brewer-Dobson Circulation index (BDC_{EHF})

176 The BDC influences TTL variability by modulating the TTL upwelling (Haynes et al.,
177 1991; Yulaeva et al., 1994; Holton et al., 1995). The deep branch of the BDC is driven by
178 extratropical stratospheric waves, which is linked to the meridional eddy heat flux in the lower
179 stratosphere (Li and Thompson, 2013). To quantify the BDC deep branch, we calculate the
180 monthly averaged zonal mean meridional eddy heat flux at 100 hPa averaged over 25°-90° in the
181 northern hemisphere minus that of the southern hemisphere (Tseng and Fu, 2017a; Randel et al.,

182 2002). We refer to this BDC index based on the eddy heat flux as BDC_{EHF} . Temperatures are
 183 correlated with wave driving during the current and previous months; thus, the BDC_{EHF} index is
 184 created using a three-month running mean centering on the previous month (Lin et al., 2009; Li
 185 and Thompson, 2013; Fu et al., 2015; Tseng and Fu, 2017a). This BDC_{EHF} index is calculated
 186 using 6 hourly ERA5 data from 2006-2021. Note that in addition to the BDC deep branch, the
 187 eddy heat flux-based index BDC_{EHF} may also include a portion of the shallow branch of the BDC
 188 (Grise and Thompson, 2013).

189 2.2.5 Partial Shallow Branch of the Brewer-Dobson Circulation index (BDC_{PSB})

190 In addition to extratropical stratospheric waves, tropical and subtropical waves also drive
 191 the TTL upwelling. The upwelling due to the subtropical waves is associated with the shallow
 192 branch of the BDC (Grise and Thompson, 2013; Abalos et al., 2014; Ortland and Alexander,
 193 2015). The shallow branch of the BDC thus also influences TTL variability by modulating the
 194 TTL upwelling. Note that in this study, the upwelling driven by equatorial planetary waves
 195 (Boehm and Lee, 2003; Deckert and Dameris, 2008; Garny et al., 2011), which is related to
 196 T500, is not considered as part of the BDC. We attempt to quantify the role of the shallow
 197 branch that may be missed by the BDC_{EHF} by using the residual TTL upwelling after removing
 198 the impacts of the QBO, T500, and BDC_{EHF} . This residual TTL upwelling which represents the
 199 partial shallow branch of the BDC is referred to as BDC_{PSB} .

200 To quantify the TTL upwelling, we calculate the upwelling at 100 hPa over 15°S-15°N
 201 using the transformed Eulerian mean (TEM) vertical velocity, for 2006-2021 using the 6-hourly
 202 ERA5 reanalysis following equation (1) (e.g., Haynes et al., 1991; Rosenlof et al., 1995; Randel
 203 et al., 2008; Abalos et al., 2012).

$$204 \quad \overline{w^*} = \overline{w} + \frac{1}{a \cos \phi} \frac{\partial}{\partial \phi} \left(\cos \phi \frac{\overline{v'T'}}{S} \right) \quad (1)$$

205 where $\overline{w^*}$ is the zonal mean TEM residual vertical velocity, \overline{w} is the zonal mean vertical
 206 velocity from ERA5, a is the radius of the earth, v is the meridional velocity, T is the
 207 temperature, and S is the stability parameter $S = \frac{HN^2}{R}$, a function of the Brunt-Vaisala frequency
 208 (N), with $H = 7$ km and $R = 287 \text{ m}^2\text{s}^{-2}\text{K}^{-1}$. Overbars and primes represent zonal means and zonal
 209 deviation respectively. After computing the upwelling, we regress out the combined impact of
 210 the QBO, T500, and BDC_{EHF} using a MLR (Garfinkel and Hartmann, 2008; Abalos et al., 2014).
 211 The 100 hPa upwelling before regressing out QBO, T500 and BDC_{EHF} has a correlation
 212 coefficient of -0.32, 0.49, and 0.46, respectively, with the QBO, T500 and BDC_{EHF} (the MLR
 213 using the QBO, BDC_{EHF} , and T500 can explain 60% of the variability in the raw 100 hPa
 214 upwelling).

215 Because this study focuses on interannual variability, all data is deseasonalized and
 216 detrended. The target variables and predictors are created as the monthly anomalies by removing
 217 the monthly climatology from June 2006 – December 2021. Before removing linear trends in
 218 each timeseries, trends are computed using linear regression and are provided in Table S1. No
 219 trend is significant at the 95% confidence level besides that of the ALLCF timeseries, but this
 220 trend is not further investigated here.

221 **3 Results**

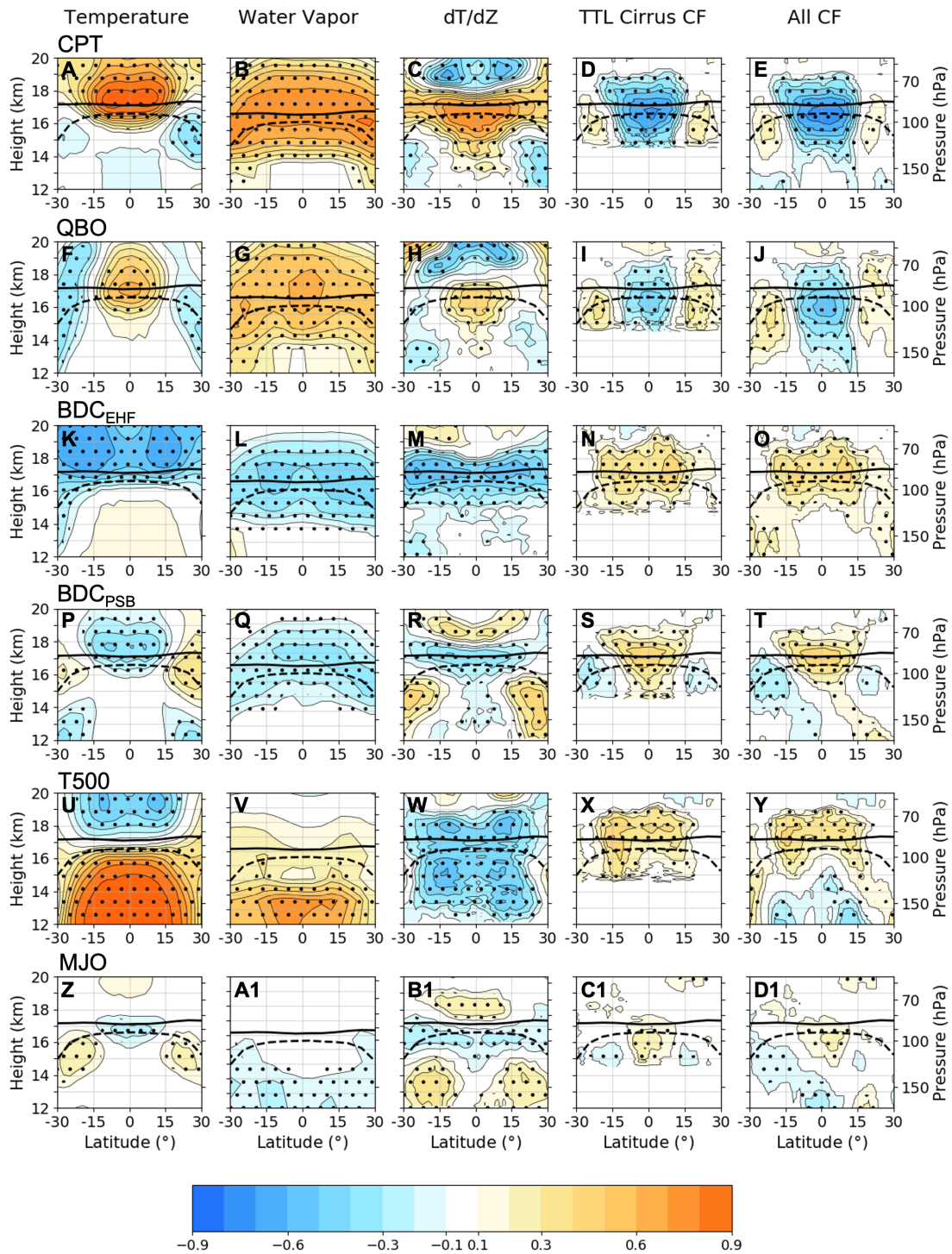
222 The climatology and interannual standard deviation of tropical upper-tropospheric and
 223 lower-stratospheric temperature, water vapor, vertical temperature gradient, and cloud fractions
 224 from June 2006 to December 2021 are provided in Figure S1. Importantly, the interannual
 225 variability for all these variables maximizes within 15°S-15°N. A significant cloud fraction
 226

227 variance occurs above the climatological cold point tropopause (Figs. S1I and S1J). Cloud
228 fraction variability above the climatological cold point tropopause may be related to coincident
229 changes in tropopause height. Figures S1 K-L show the interannual variance in a vertical
230 coordinate relative to the cold point tropopause height, showing cloud fraction variability to
231 maximize below the cold point tropopause.
232

233 **3.1 Target Variable Correlations with Modes of Large-Scale Variability**

234 Figure 1 shows the correlation between target variables with the zonal mean cold point
235 tropopause temperature (CPT) averaged over 15°S-15°N (row 1), and the correlations of target
236 variables with the modes of large-scale variability (row 2-6). Although the CPT is not a mode of
237 variability, it is critically important for stratospheric water vapor (e.g., Randel and Jensen, 2013)
238 and is highly correlated with TTL cirrus cloud fraction (Tseng and Fu, 2017a). CPT is
239 significantly correlated with stratospheric temperatures but has little correlation with those in the
240 troposphere (Fig. 1A), suggesting that processes controlling the CPT also impact the tropical
241 lower stratosphere (Randel and Wu, 2015). Lower-stratospheric water vapor reaches correlations
242 of ~0.8 at the cold point tropopause (Fig. 1B), indicative of the temperature control of lower-
243 stratospheric water vapor. Water vapor is transported vertically into the stratosphere over the
244 tropics by the BDC (Brewer et al., 1949; Mote et al., 1996; Flury et al., 2012; Flury et al., 2013),
245 and is also transported between lower and higher latitudes through quasi-horizontal isentropic
246 mixing (Randel and Park, 2019). These processes are responsible for the convex shape of peak
247 correlations between CPT and water vapor in the TTL (Fig. 1B). CPT is strongly anticorrelated
248 with equatorial TTL cirrus and All cloud fraction (Figs. 1D-E). Positive correlations between
249 CPT and cloud fraction exist near the subtropical lapse rate tropopause, the inverse of the
250 correlation between CPT and subtropical temperature. The strong correlations between CPT and
251 the target variables stress the temperature control of the water partitioning between vapor and
252 clouds in the TTL. Correlations between the CPT and target variables extends to higher latitudes
253 in Figure S2.

254



255
 256 Figure 1: Correlations in tropical upper troposphere and lower stratosphere between target
 257 variable monthly anomalies and modes of the large-scale variability, except for row 1 that shows
 258 correlation between target variables and cold point temperature (CPT) averaged over 15°S-15°N.
 259 Stippling indicates significance at 95% confidence and the solid (dashed) black line is the
 260 climatological mean cold point (lapse rate) tropopause.
 261

262 The QBO and temperature are correlated in the equatorial TTL, but anticorrelated in the
 263 subtropical TTL due to the QBO's meridional circulation (Fig. 1F) (Plumb and Bell, 1982;
 264 Baldwin et al., 2001; Pahlavan et al., 2021). QBO correlations with cloud fraction are inverse to
 265 those of temperature (Fig. 1I-J). Subtropical cloud fraction correlations are weaker than the
 266 equatorial signal, possibly due to the weaker QBO-temperature correlations and the lower
 267 relative humidity. Significant QBO correlations with All cloud fraction reach into the
 268 troposphere as low as ~ 13 km (Fig. 1J), below the region of peak QBO power (Sweeney et al.,
 269 2023). This deep QBO signature may be due to convective feedbacks (Tegtmeier et al., 2020).
 270 The QBO and water vapor correlations peak at the equatorial tropopause and are spread
 271 latitudinally due to quasi-isentropic mixing (Fig. 1G). The QBO impacts lapse-rate tropopause
 272 temperature out to near 50° in both hemispheres with weak statistically significant implications
 273 for cloud fraction (Fig. S2).

274 Increases in BDC_{EHF} cause upwelling and cooling in the tropical lower stratosphere (Fig.
 275 1K) (Mote et al., 1996; Plumb and Eluszkiewicz, 1999; Randel et al., 2002). Decreasing
 276 temperature and vertical temperature gradient promotes cloud formation at and above the
 277 climatological mean tropopause (Figs. 1N-O). Notably, temperature and CPT correlations can be
 278 largely inferred from temperature and QBO minus temperature and BDC_{EHF} , both in the TTL
 279 (i.e., Fig. 1A resembles Fig. 1F minus Fig. 1K), and globally (Fig. S2).

280 The BDC_{PSB} index is related to the TTL cold anomalies flanked by subtropical upper-
 281 tropospheric warm anomalies (Fig. 1P), with tropospheric cold anomalies underneath the warm
 282 anomalies. BDC_{PSB} is also anticorrelated with lower-stratospheric water vapor (Fig. 1Q).
 283 BDC_{PSB} cloud fraction correlations peak near the equatorial tropopause (Figs. 1S-T). The
 284 BDC_{PSB} and temperature correlation pattern resembles the temperature tendencies caused by
 285 subtropical upper-tropospheric waves which can cause subseasonal variability in the shallow
 286 branch of the BDC (Grise and Thompson, 2013; Abalos et al., 2014). The shallow branch of the
 287 BDC is also driven by subtropical stratospheric waves, which is considered in BDC_{EHF} (Grise
 288 and Thompson, 2013). Figures 1P-T show that BDC_{PSB} is well correlated with the target
 289 variables and is an important component of TTL variability.

290 T500 measures tropospheric temperature and is positively correlated with temperatures
 291 below the tropopause (Fig. 1U). Increased T500 dynamically induces upwelling and cooling of
 292 the lower stratosphere (Randel et al., 2009; Calvo et al., 2010; Shepard and McLandress, 2011;
 293 Lin et al., 2017). The net result of warming below the tropopause and cooling above is a
 294 reduction of vertical temperature gradient throughout the TTL (Fig. 1W). T500 has significant
 295 correlations with cloud fraction near and above the climatological tropopause (Davis et al., 2013;
 296 Avery et al., 2017; Ye et al., 2018). The correlation between T500 and lower-stratospheric water
 297 vapor is insignificant (Fig. 1V), consistent with T500's weak impact on CPT ($r=-0.11$) (Liang et
 298 al., 2011; Konopka et al., 2016; Diallo et al., 2018; Garfinkel et al., 2021; Ziskin Ziv et al.,
 299 2022). This may be expected given that much of the T500 variability is related to ENSO which
 300 shows a strong longitudinal dipole impact on CPT which cancels in the zonal mean (Randel et
 301 al., 2000; Scherllin-Pirscher et al., 2012; Tseng and Fu, 2017a; Garfinkel et al., 2021).
 302 Interpreting the physical mechanism by which T500 influences the CPT is complicated due to
 303 competing processes, but it is important to understand the response of stratospheric water vapor
 304 to global warming. Discussion of the relevant mechanisms by which T500 may impact the TTL
 305 is provided in Section 3.3. The correlation between T500 and global temperature (Fig. S2)
 306 reveals a meridional circulation in the tropical and subtropical lower stratosphere.

307 The last row in Fig. 1 shows correlations between the MJO and target variables. The
308 MJO is the main mode of intraseasonal variability in the tropics (Madden and Julian, 1971), and
309 impacts subseasonal variability of temperature and cloud fraction in the TTL (Virts and
310 Wallace., 2014; Virts et al., 2010). MJO-temperature correlations have a distinct pattern of weak
311 equatorial (subtropical) anticorrelation (correlation) (Grise and Thompson, 2013). Results of Fig.
312 1 show that the MJO only weakly correlates with the TTL target variables. This is partly because
313 the monthly averaging of the MJO index and target variables smooths the intraseasonal
314 variability.

315

316 **3.2 Explained Variances in Target Variables from MLR**

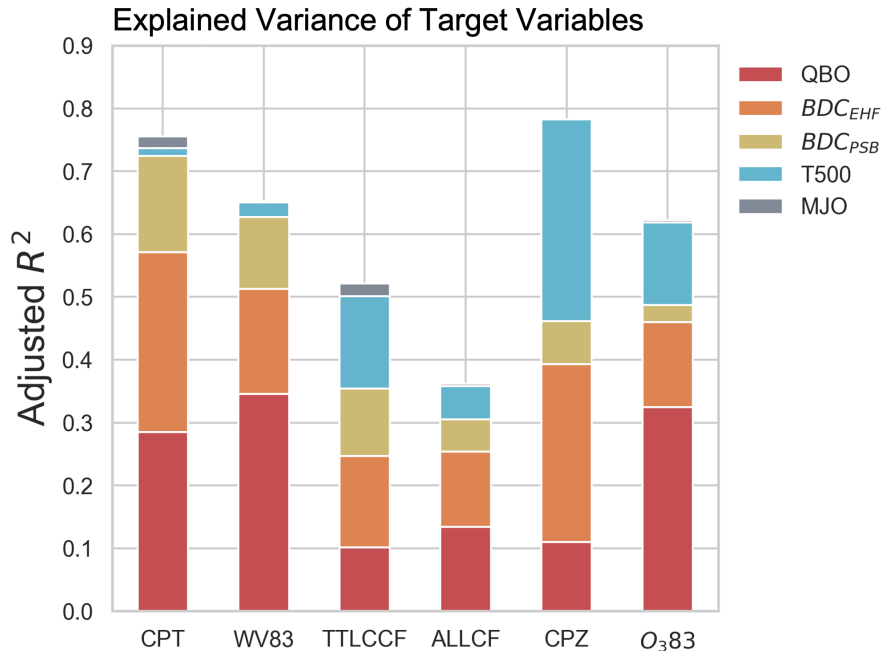
317 We next use the modes of the large-scale variability as predictors in a multiple linear
318 regression (MLR) to quantify the explained variance of cold point tropopause temperature
319 (CPT), water vapor at 83 hPa (WV83), cold point tropopause height (CPZ), ozone concentrations
320 at 83 hPa (O₃83), total TTL cirrus cloud fraction (TTLCCF), and All cloud fraction (ALLCF), all
321 averaged over 15°S-15°N.

322 Explained variance is quantified using the adjusted R², which accounts for artificial
323 inflation due to collinearity in the MLR and is always smaller than the true R². The unique
324 contribution of explained variance to the adjusted R² from each predictor is not possible unless
325 predictors are independent of each other. A correlation matrix among all predictors and target
326 variables is provided in Figure S3. The predictors show small correlations with each other over
327 the period investigated, which are all statistically insignificant. For example, the correlation is -
328 0.07 between QBO and BDC_{EHF}, and 0.14 between T500 and BDC_{EHF}. To account for these non-
329 zero correlations, we partition the adjusted R² into the unique contributions from the QBO,
330 BDC_{EHF}, BDC_{PSB}, T500, and MJO by recursively adding each predictor to our MLR model while
331 also permuting the order of addition. This allows for an estimate of unique explained variance
332 (Lindeman et al., 1980). We note that this method is not perfect because the predictors are not
333 entirely independent but provides an estimate of the unique explained variance from each mode
334 of variability.

335 Figure 2 shows the MLR's explained variance of CPT (76%), WV83 (65%), TTLCCF
336 (52%), ALLCF (36%), CPZ (78%), and O₃83 (62%). Stratospheric processes (i.e., the QBO,
337 BDC_{EHF}, and BDC_{PSB}) dominate the variance captured in CPT, WV83, and ALLCF. T500
338 contributes more to TTLCCF and O₃83, and to nearly half of the explained variance in CPZ. The
339 MJO minimally affects any target variable. BDC_{PSB} explains substantial variances in CPT,
340 WV83, and TTLCCF, and should be considered an important component of the TTL variability.
341 The MLR here significantly enhances explained variance of CPT and TTLCCF compared to
342 previous studies (Tseng and Fu, 2017a) by considering BDC_{PSB}.

343

344

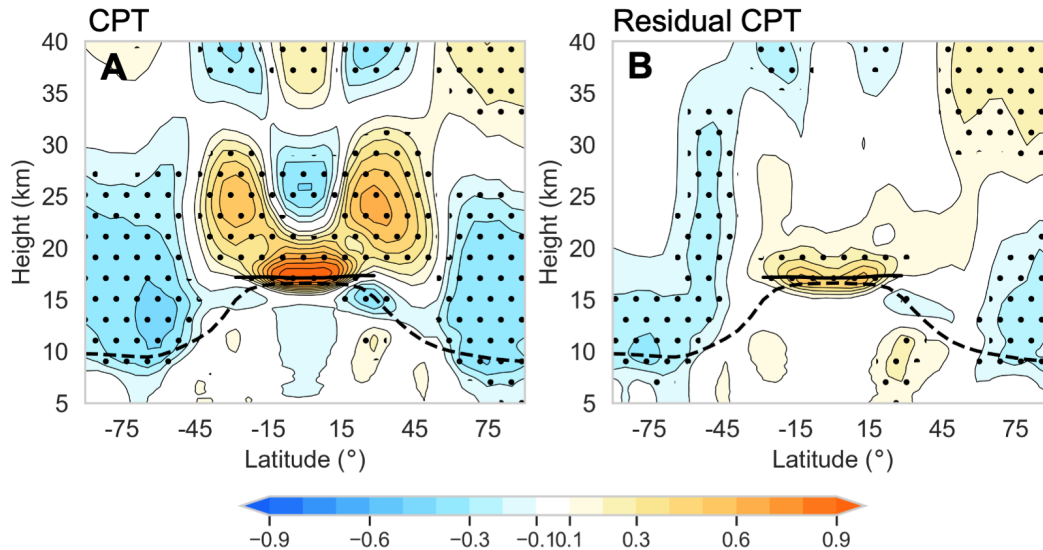


345
346 Figure 2: Adjusted R^2 from multiple linear regression model applied to target variables using
347 modes of the large-scale variability as predictors. Colored sections indicate the estimated
348 contribution to the adjusted R^2 from each predictor.
349

350 Tseng and Fu (2017a) stressed the importance of CPT for TTLCCF variability. A linear
351 regression using only CPT as a predictor explains 41% of TTLCCF variance, while the MLR in
352 Fig. 2 explains 52%. Including CPT as an additional predictor in the MLR for TTLCCF only
353 increases the explained variance slightly from 52 to 54%, indicating that most of the CPT control
354 of TTLCCF has already been included in our MLR. But this is not true for WV83 whose
355 explained variance increases by 8% (from 65% to 73%) when including CPT as an additional
356 predictor. Thus, a better understanding of the CPT variance would help explain WV83 variance.
357 The cloud fraction explained variance is strongly dependent on altitude, where at 17 km the
358 MLR explains over 60% of the variance in TTL cirrus and All cloud fraction, possibly due to the
359 higher frequency of laminar tropopause cirrus at these altitudes (Wang et al., 2019).

360 TTL ozone variability is primarily due to the TTL upwelling and in-mixing of ozone
361 depleted tropospheric air (Randel et al., 2007; Konopka et al., 2009; Solomon et al., 2016; Wang
362 and Fu, 2021; Wang and Fu, 2023). Long-term ozone concentrations at a fixed height in the TTL
363 may decrease due to the strengthening of the tropical upwelling associated with the BDC, and/or
364 tropospheric expansion due to warming (Banerjee et al., 2016; Chiodo et al., 2018; Wang et al.,
365 2020; Match and Gerber, 2022). Fig. 2 shows that the MLR explains 62% of O_{383} variance, with
366 about half attributed to the QBO while the rest is split roughly equally between BDC_{EHF} and
367 T500. Despite the QBO's important role in determining O_{383} , decadal changes in O_{383} due to
368 the QBO are uncertain due to ambiguity in the QBO response to global warming (e.g., Richter et
369 al., 2020; Fu et al. 2020). Our results suggest that both T500 and the BDC_{EHF} affect O_{383} (Match
370 and Gerber, 2022). However, the T500 influence on O_{383} may operate via a dynamic response in
371 the TTL upwelling. Further discussion on T500's impact on target variables including O_{383} , can
372 be found in Section 3.3.

373 A key result of Fig. 2 is that despite the strong correlation between CPT and CPZ ($r=-$
 374 0.74) the interannual variability of CPT is predominately explained by stratospheric processes,
 375 while CPZ's variability is equally explained by stratospheric and tropospheric processes. In
 376 Figure 3, we further examine how CPT covaries with the tropospheric and stratospheric
 377 temperatures. Fig. 3A illustrates the correlations of zonal mean temperature from 5-40 km over
 378 90°S-90°N obtained from the RO data with CPT. Fig. 3B shows the correlations of zonal mean
 379 temperature and the residual CPT after removing all variance captured by the MLR in Fig. 2.



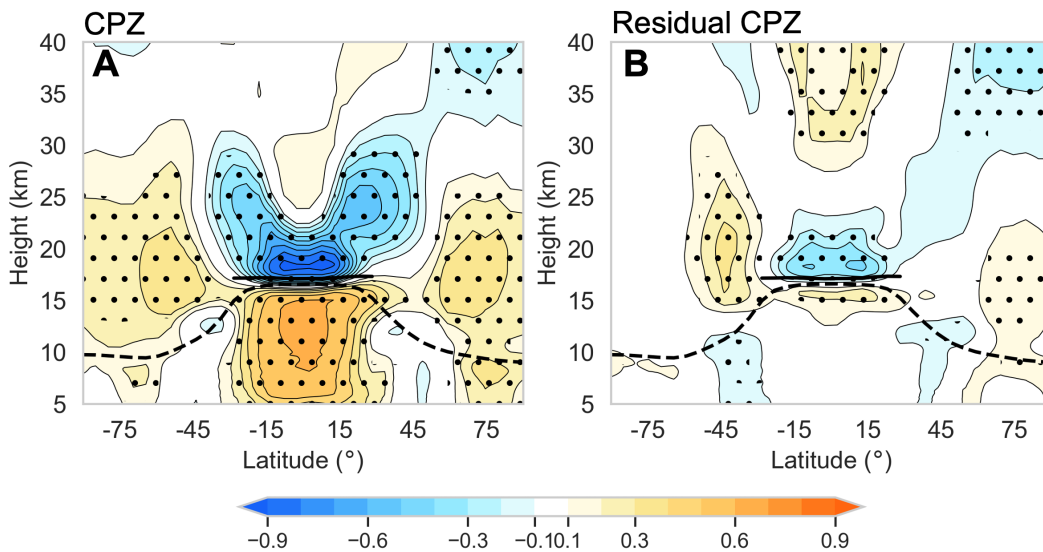
380
 381 Figure 3: Correlation of zonal mean temperature globally from 5-40 km with (A) cold point
 382 temperature averaged over 15°S-15°N (CPT), and (B) residual CPT after regressing out all
 383 modes of large-scale variability using the MLR shown in Fig. 2. Stippling indicates significance
 384 at 95% confidence and the solid (dashed) black line is the climatological mean cold point (lapse
 385 rate) tropopause.

386
 387 CPT is strongly correlated with temperatures throughout the global stratosphere, but not
 388 with those of the troposphere, as seen in Fig. 3A, consistent with the dominant role of
 389 stratospheric processes in CPT variance. The checkerboard pattern in the tropical stratosphere is
 390 due to the QBO's meridional circulation (Baldwin et al., 2001). The out of phase correlation
 391 above the equatorial cold point and the polar lower stratosphere is due to the BDC's meridional
 392 circulation. Regressing the modes of large-scale variability out of the CPT significantly reduces
 393 its covariability with stratospheric temperatures (Fig. 3B).

394 Fig. 3B shows that residual CPT is still correlated (anticorrelated) near the equatorial
 395 tropopause (polar lower stratosphere). This correlation pattern with the residual CPT is
 396 reminiscent of the global correlations expected from the BDC, which is surprising given that the
 397 QBO, BDC_{EHF} , BDC_{PSB} , T500, and MJO have all been regressed out. Note that both the CPT
 398 variability and that of zonal mean temperature throughout the global upper troposphere and
 399 lower stratosphere are derived from RO data, whereas the BDC_{EHF} and BDC_{PSB} indices are
 400 derived from ERA5 (see Section 2.2). Thus, this pattern of residual variability may be partly
 401 caused by reanalysis errors in representation of the BDC.

402 Figure 4 shows the correlations between zonal mean temperature with CPZ. In contrast to
 403 CPT, the CPZ is also highly correlated with temperature in the tropical troposphere (Fig. 4A).
 404 Increased tropospheric temperatures raise CPZ through thermal expansion of the troposphere in

405 addition to dynamical upwelling. T500 contributes to nearly half of the interannual variance in
 406 CPZ (see Fig. 2), which is relevant for future increases in the CPZ in response to the T500
 407 increase (Santer et al., 2003; Lorenz and DeWeaver, 2007). The stark differences in correlation
 408 patterns of CPT versus that of CPZ (Fig. 3A and 4A) may help validate model representations of
 409 tropical tropopause characteristics. After regressing out all modes of variability from CPZ the
 410 correlation patterns with temperature are still connected to the global stratosphere (Fig. 4B),
 411 which again indicates a potential issue in the indices used to represent the stratospheric
 412 processes.

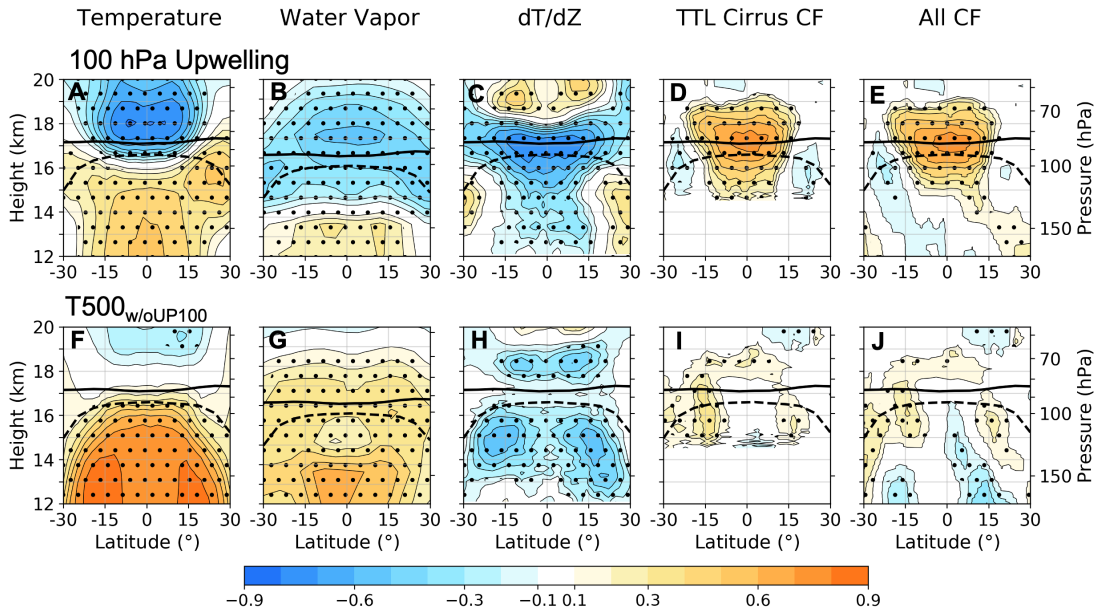


413
 414 Figure 4: Same as Fig. 3, but for cold point tropopause height (CPZ).
 415

416 3.3 Isolating the Role of the TTL Upwelling and Thermodynamics

417 The large-scale modes used as predictors in this study can impact TTL variability by
 418 modulating the TTL upwelling. This upwelling helps shape temperatures of the region through
 419 adiabatic cooling and, to a smaller extent, cloud formation and the transport of radiatively active
 420 species (Corti et al., 2006; Abalos et al., 2012; Birner and Charlesworth, 2017). On the other
 421 hand, T500 could also impact the TTL through thermodynamic processes in addition to
 422 upwelling. Here we examine the role of the dynamic upwelling and thermodynamic processes.

423 To assess the upwelling's impact on TTL variability, we use the original 100 hPa TEM
 424 upwelling from 15°S-15°N as described in Section 2.2. Correlations between this index and the
 425 target variables are shown in Figures 5A-E. The 100 hPa upwelling is positively correlated with
 426 tropospheric temperatures and negatively correlated with lower-stratospheric temperatures (Fig.
 427 5A). The 100 hPa upwelling is strongly anticorrelated with CPT ($r=-0.68$) and is also
 428 anticorrelated with TTL water vapor (Fig. 5B). Upwelling also increases cloud fractions (Figs.
 429 5D and 5E), mediated by the reductions in near tropopause temperature and vertical temperature
 430 gradient (Figs. 5A and 5C). TTLCCF has a correlation with the 100 hPa upwelling of $r=0.69$.
 431 Thus, regressing only this upwelling onto TTLCCF can explain 47% of the variability, close to
 432 what the MLR with all predictors can (52% shown in Fig. 2). Since most of the TTLCCF
 433 variance captured by the full MLR is explained using just the 100 hPa upwelling, it is suggested
 434 that the modes of the large-scale variability control TTL cirrus clouds by modulating the 100 hPa
 435 upwelling.



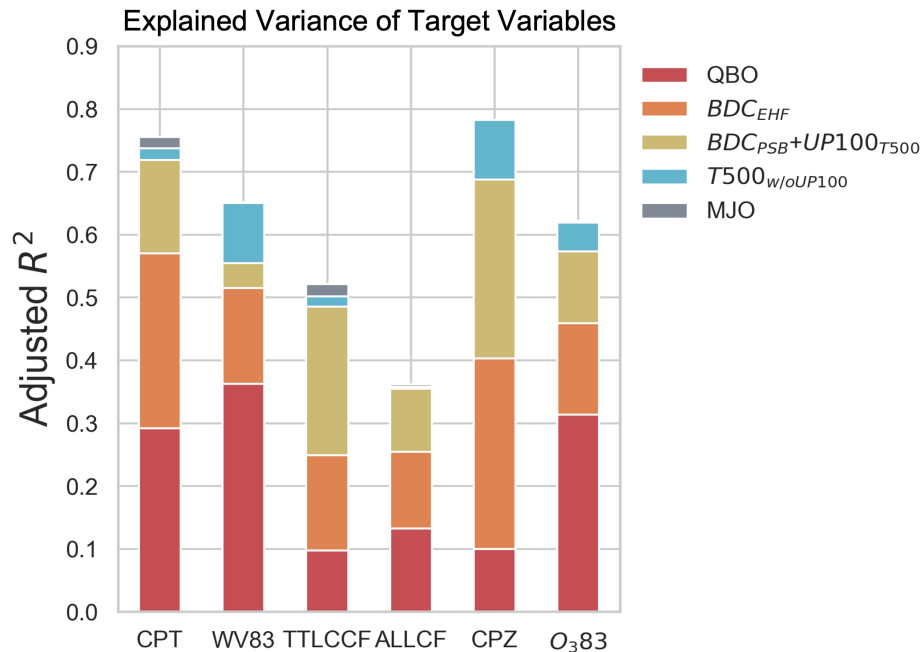
436
 437 Figure 5: As Fig. 2 but A-E show correlations of target variables with the 100 hPa upwelling. F-J
 438 shows correlations with $T500_{w/oUP100}$ (i.e., T500 after regressing out the 100 hPa upwelling,
 439 QBO, and BDC_{EHF}).
 440

441 Temperature and 100 hPa upwelling correlations in Fig. 5A are reminiscent of
 442 temperature and T500 correlations shown in Fig. 1U, but with stronger (weaker) correlations in
 443 stratosphere (troposphere). T500 is well correlated with the 100 hPa upwelling ($r=0.49$) and can
 444 influence the target variables by modulating the upwelling. T500 may induce upwelling through
 445 eddy momentum flux convergence in the tropical upper troposphere driven by convective latent
 446 heating (Boehm and Lee, 2003). However, T500 may also impact the target variables through
 447 thermodynamic processes such as radiative heating of the TTL, tropical tropospheric expansion,
 448 tropical convection, and/or other physical processes (Lin et al., 2017). We next attempt to isolate
 449 the T500 thermodynamic effects using regression analysis. It might be difficult to do so by just
 450 using the regression analysis given that the dynamic and thermodynamic processes may be
 451 closely coupled, yet this analysis may still provide valuable insights. We urge further modelling
 452 studies to validate results shown here.

453 To remove T500's dynamic contribution to TTL variability, we regress the 100 hPa
 454 upwelling out of T500. In addition to the 100 hPa upwelling, the QBO and BDC_{EHF} indices are
 455 also removed from T500. Since the impact of removing the QBO and BDC_{EHF} is small due to
 456 minimal correlations with T500 (Fig. S3), we refer to this T500 index without the dynamic
 457 components as $T500_{w/oUP100}$ (which can be considered as the T500 thermodynamic index).
 458 Figures 5F-J show the correlation coefficients between $T500_{w/oUP100}$ with target variables. Fig. 5F
 459 shows warming below the tropopause and little to no cooling in the stratosphere as would be
 460 expected after removing the dynamically induced response to T500. While significant positive
 461 tropospheric temperature correlations in Fig. 5F reach closer to the equatorial cold point
 462 tropopause than those with the original T500 index shown in Fig. 1U, no statistically significant
 463 correlation between $T500_{w/oUP100}$ and CPT exists ($r=0.15$). Given that the 100 hPa upwelling
 464 explains most of the TTLCCF variability, removing its influence from T500 also largely removes
 465 its influence on TTL cirrus clouds (Figs. 5I and 5J).

466 Notably, $T500_{w/oUP100}$ shows a significant correlation with lower-stratospheric water
 467 vapor (Fig. 5G). This is in stark contrast to results of Fig. 1V, where the T500 index showed no
 468 significant impact on lower-stratospheric water vapor. Fig. 5G may suggest that $T500_{w/oUP100}$
 469 covaries with lower-stratospheric water vapor, but this covariability is damped by coincident
 470 cooling due to the TTL upwelling caused by T500. While $T500_{w/oUP100}$ is correlated with lower-
 471 stratospheric water vapor, it is not significantly correlated with CPT. Thus, the $T500_{w/oUP100}$
 472 impact on lower-stratospheric water vapor might not work through a simple increase in CPT but
 473 may instead be related to $T500_{w/oUP100}$'s impact on the TTL environment where dehydration,
 474 convective evaporation, subtropical water vapor in-mixing, and/or other uninvestigated processes
 475 occur (Dessler et al., 2013; Ye et al., 2018; Bourguet and Linz, 2023).

476 The differences between Figs. 1U-Y and Figs. 5F-J suggest that T500 contributes to TTL
 477 variability partly through changes in the 100 hPa upwelling. Figure 6 is the same as Fig. 2 but
 478 replaces T500 with $T500_{w/oUP100}$ and BDC_{PSB} with $BDC_{PSB}+UP100_{T500}$. $BDC_{PSB}+UP100_{T500}$ is
 479 the combination of BDC_{PSB} and the 100 hPa upwelling induced by T500, which is computed in
 480 the same way as BDC_{PSB} but without regressing out T500 (see Section 2.2). This replacement is
 481 to group the T500 that is linearly related to the 100 hPa upwelling ($UP100_{T500}$) with the BDC_{PSB}
 482 and then isolate the T500 that is not linearly related to the 100 hPa upwelling ($T500_{w/oUP100}$).



483 Figure 6: Same as Fig. 2, but the $BDC_{PSB}+UP100_{T500}$ is the BDC_{PSB} without removing the
 484 influence of T500, i.e., the contribution from BDC_{PSB} and the 100 hPa upwelling due to T500
 485 ($UP100_{T500}$). $T500_{w/oUP100}$ is the T500 index after regressing out the original 100 hPa upwelling,
 486 the QBO, and BDC.
 487
 488

489 This replacement does not impact the total explained variance, and small changes in
 490 explained variances by QBO, BDC_{EHF} and MJO result from changes in collinearities. Figure 6
 491 shows that $T500_{w/oUP100}$ contributes minimally to explained variance of TTLCCF and ALLCF
 492 because cloud fraction variance is tightly coupled to the TTL upwelling. While Fig. 2 showed
 493 that T500 contributes nearly half of the explained variance in CPZ, Fig. 6 shows that
 494 $T500_{w/oUP100}$ contributes much less to the explained variance in CPZ. Figures 2 and 6 suggest that

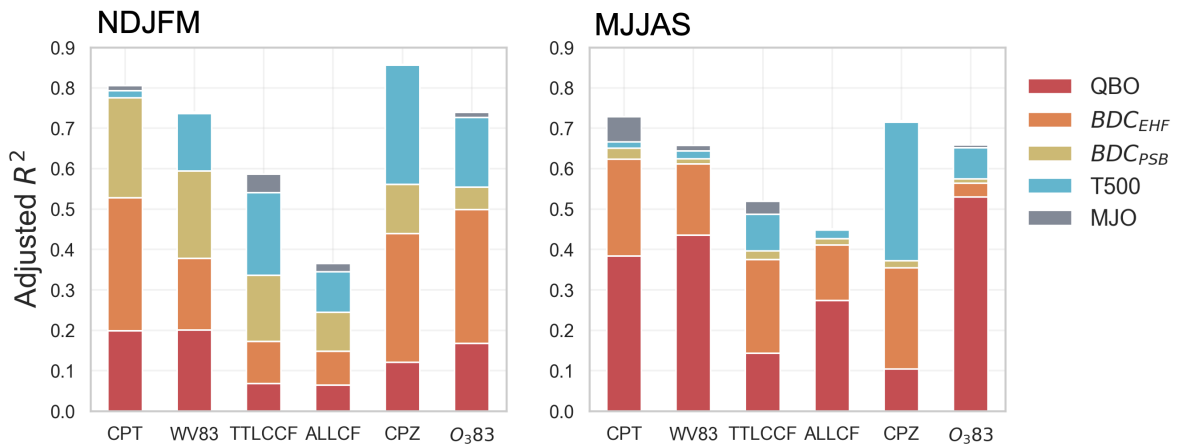
495 more than 2/3 of the T500 control of CPZ is through T500's induced upwelling (Austin and
 496 Reichler, 2008). Similarly, only about 1/3 of explained O₃83 variance by T500 (Fig.2) comes
 497 from T500_{w/oUP100} (Fig.6).

498 In contrast, Fig. 6 shows an enhanced role of T500_{w/oUP100} in WV83 variance relative to
 499 T500 in Fig. 2. The T500_{w/oUP100} influence on WV83 may be important for climate feedbacks due
 500 to the important role of lower-stratospheric water vapor (Solomon et al., 2010). Finally it is
 501 worth noting that the explained CPT variances by BDC_{PSB} (Fig.2) and BDC_{PSB}+UP100_{T500} (Fig.
 502 6) are almost identical, indicating that both UP100_{T500} and T500_{w/oUP100} have little impacts on
 503 CPT.
 504

3.4 Seasonality

506 The seasonal influence of large-scale modes on TTL variability is less studied.
 507 Correlation between CPT and lower-stratospheric water vapor is strongest in boreal winter
 508 (Randel and Jensen, 2013; Randel and Park, 2019; Lu et al., 2020). Seasonal changes in the
 509 tropical upwelling and the Asian monsoon also impact TTL variability (Sunilkumar et al., 2010;
 510 Randel et al., 2007; Randel et al 2010; Walker et al., 2015; Ueyama et al., 2015; Ueyama et al.,
 511 2018; Das and Suneeth, 2020). Modes of the large-scale variability may also impact the target
 512 variables differently throughout the year (Li and Thompson, 2013; Konopka et al., 2016; Tweedy
 513 et al., 2018; Martin et al., 2021; Sweeney et al., 2023). Here, we examine how these modes of
 514 variability impact the target variables during extended boreal winter (November-March;
 515 NDJFM) and extended boreal summer (May-September; MJJAS). During NDJFM the TTL is
 516 colder, drier, and has more TTL cirrus than in MJJAS (Figure S4). During MJJAS, lower
 517 stratospheric water vapor increases (Fig. S4G) and All cloud fraction maximizes (Fig. S4J) in the
 518 northern hemisphere TTL due to the Asian Summer Monsoon (e.g., Santee et al., 2017).
 519 Regardless of season, interannual variance is strongest near the equator (Fig. S4).

520 The MLR used in Fig. 2 is fit in both NDJFM and MJJAS individually in Figure 7.
 521 Figure S5 shows correlation matrices between all target variables and predictors for both
 522 NDJFM and MJJAS separately. The MLR predicts all target variables better during NDFJFM than
 523 MJJAS, except ALLCF. Note that the partitioning of explained variance is less reliable after
 524 splitting the data based on season because of collinearities between the modes of variability, and
 525 smaller number of degrees of freedom.



526
 527 Figure 7: Adjusted R² from MLR model applied to target variables for NDJFM and MJJAS
 528 individually. Colored sections indicate the contribution to the adjusted R² from each predictor.
 529

530 Fig. 7 highlights the increased QBO influence during MJJAS for all variables except
 531 CPZ: CPT ($r=0.5$ in NDJFM and $r=0.61$ in MJJAS), WV83 (0.53 in NDJFM and 0.66 in
 532 MJJAS), TTLCCF ($r=-0.26$ in NDJFM and $r=-0.36$ in MJJAS), ALLCF ($r=-0.26$ in NDJFM and
 533 -0.51 in MJJAS), and O_383 ($r=0.43$ in NDJFM and $r=0.72$ in MJJAS). This is despite the
 534 stronger QBO-MJO connection and lower-stratospheric temperature impact during boreal winter
 535 (Yoo and Son, 2016; Tegtmeier et al., 2020; Martin et al., 2021). A seasonality in the QBO's
 536 descent has been well documented (Dunkerton, 1990; Coy et al., 2020). Seasonal changes in the
 537 QBO's explained variance may be a result of a seasonality in the zonal symmetry of the QBO
 538 impact on the TTL (Tegtmeier et al., 2020). The MJJAS TTL is less variable than that of
 539 NDJFM (compare rows 3 and 4 of Fig. S4), so an equally large QBO signal should be more
 540 salient during this season.

541 The BDC_{EHF} TTL impact maximizes during boreal winter due to increased extratropical
 542 stratospheric wave driving (Yulaeva, et al., 1994). NDJFM BDC_{EHF} impacts are larger for CPT,
 543 CPZ, and O_383 . The BDC_{EHF} impact on WV83 is comparable during both seasons, but this result
 544 is complicated by the strength of the BDC_{EHF} during the two seasons and thus the time of transit
 545 between the CPT and 83 hPa (Randel and Park, 2019). WV83 results of Fig. 7 are lagged by one-
 546 month (see section 2.1). Removing this one-month lag reveals the much stronger BDC_{EHF} control
 547 of WV83 during NDJFM compared to MJJAS. We find that the BDC_{EHF} explanation of TTL
 548 cirrus clouds is larger during MJJAS (correlation between BDC and TTLCCF is $r=0.39$ in
 549 NDJFM and $r=0.51$ in MJJAS). This is surprising given the strong connections between the
 550 boreal winter BDC_{EHF} and TTL cirrus clouds previously reported (Li and Thompson, 2013), but
 551 is not studied further here. Increased explained variance of target variables during NDFJM is
 552 partly due to the role of BDC_{PSB} . Although the seasonal cycle in the BDC_{PSB} index has been
 553 removed, anomalies are weaker during MJJAS. This may be related to stronger subtropical wave
 554 driving variability during NDJFM (Randel et al., 2008; Ortland and Alexander, 2014).

555 T500's impact on the target variables is stronger in NDJFM for WV83, TTLCCF,
 556 ALLCF, and O_383 . This increase in the tropospheric influence on the TTL variability during
 557 these seasons may be related to seasonality in ENSO activity or tropical wave activity captured
 558 by the T500 index (Ortland and Alexander, 2014; Garfinkel et al., 2018). The seasonality of the
 559 MJO impact on the target variables is more inconsistent and may be further complicated due to
 560 aliasing of the Boreal Summer Intraseasonal Oscillation into our MJO index.

561

562 **4 Discussion and Conclusions**

563 Stratospheric water vapor and TTL cirrus clouds are important components of the climate
 564 system but poorly constrained in models. Both exhibit large interannual variability and are linked
 565 by temperature in the TTL (Jensen et al., 2013; Tseng and Fu, 2017a). The QBO, BDC_{EHF} ,
 566 BDC_{PSB} , T500, and MJO contribute to this interannual variability by modulating the dynamic
 567 and thermodynamic environment of the TTL (e.g., Dessler et al., 2013; Davis et al., 2013;
 568 Randel and Wu, 2015). Multiple linear regressions (MLRs) with modes of the large-scale
 569 variability as predictors have been used to study the temperature control of water vapor and TTL
 570 cirrus clouds (Dessler et al., 2014; Austin and Reichler, 2008; Oman et al., 2008; Garfinkel et al.,
 571 2018). Here we synthesize these results by applying a MLR to CPT, WV83, and TTLCCF and
 572 further previous efforts by applying the MLR to ALLCF, CPZ, and O_383 .

573 The MLR explains significant amounts of variance in CPT (76%), WV83 (65%),
 574 TTLCCF (52%), ALLCF (36%), CPZ (78%), and O_383 (62%). Decomposing the explained
 575 variance by predictor reveals that for all variables the stratospheric processes explain a larger

576 fraction of the variance. A strong stratospheric predictor of the target variables which received
577 little attention in previous studies is BDC_{PSB} . Temperature and BDC_{PSB} correlations have a
578 distinct pattern (see Fig. 1P) reminiscent of temperature tendencies caused by subtropical wave
579 driving (Randel et al., 2008; Grise and Thompson, 2013; Abalos et al., 2014). Future work
580 should identify the source of variability of BDC_{PSB} , as it is a significant source of TTL
581 variability. To our knowledge, this is also the first study to show the observed connection
582 between the tropical cold point tropopause temperature and height and global tropospheric and
583 stratospheric temperatures.

584 Nearly all explained CPT variability comes from the QBO, BDC_{EHF} , and BDC_{PSB} (see
585 Fig. 2). Notably, CPT is not correlated with tropical tropospheric temperatures (Fig. 3A). In
586 contrast CPZ is controlled by near equal contributions from stratospheric and tropospheric
587 processes. The robust correlation between CPT (CPZ) and stratospheric (stratospheric and
588 tropospheric) temperatures shown in Fig. 3A (Fig. 4A) can be used to validate model
589 representations of tropopause characteristics. GCM simulations suggest that CPZ and CPT
590 increase in response to warming (Austin and Reichler, 2008; Gettelman et al., 2009; Gettelman
591 et al., 2010; Hardiman et al., 2015; Lin et al., 2017; Wang and Fu, 2023). To the extent that
592 interannual responses to T500 increases can be compared with model simulations of surface
593 warming, observed interannual variability is consistent with model simulations for the CPZ
594 response to tropospheric warming, but not for the CPT response (Lin et al., 2017).

595 T500 can dynamically induce TTL upwelling. However, T500 can also impact the TTL
596 through thermodynamic processes not directly tied to the upwelling (Lin et al., 2017; Ye et al.,
597 2018; Bourguet and Linz, 2023). To isolate the dynamical impact of T500, the T500 index was
598 separated into the part that was linearly related to the 100 hPa upwelling and that which was not.
599 Our results suggest that the primary influence of T500 on TTLCCF, ALLCF, CPZ and O_383 is
600 via the dynamically induced upwelling (comparing Figs. 6 and 2). Notably, the T500 index that
601 is independent of the TTL upwelling is significantly correlated with lower-stratospheric water
602 vapor (Fig. 5G) which may be relevant for climate feedbacks (Dessler et al., 2013). While T500
603 is expected to increase with greenhouse gas concentrations, its interannual variability is greatly
604 influenced by ENSO that is associated with specific SST pattern changes, and thus conclusions
605 relevant to climate change drawn from the results shown here need to be validated by modeling
606 studies.

607 Because of the CPT's central role in stratospheric water vapor and TTL cloud fraction, it
608 is critically important to understand its interannual variability. The correlation patterns between
609 temperature and residual CPT (after regressing out all modes of variability) still resemble the
610 BDC, with positive (negative) correlations near the tropical (polar) lower stratosphere (Fig. 3B).
611 Given that we regressed out both the BDC_{EHF} and BDC_{PSB} indices, this residual CPT correlation
612 resembling the BDC is surprising. Zonal mean temperature data and the CPT timeseries used in
613 Fig. 3A comes from RO observations, whereas the BDC_{EHF} and BDC_{PSB} indices come from
614 ERA5, and thus the residual correlation pattern may result from the tropical upwelling
615 quantification from reanalysis. The residual variability in WV83 and O_383 is also correlated with
616 the global stratosphere (Figure S6). Future work should thus aim to better understand this
617 dynamical influence of the stratospheric circulation on the CPT.

618
619 **Acknowledgments**

620 This research is supported by the NASA FINESST Grant 80NSSC22K1438 and NSF Grant
621 AGS-2202812. Additional funding was provided by the Calvin Professorship in Atmospheric
622 Sciences. We thank Prof. John M. Wallace and Mingcheng Wang for their valuable discussions
623 regarding the paper. We also thank the two anonymous reviewers for their help in shaping the
624 scope of the paper, and Stephen Bourguet for his insight and thoughtful comments which were
625 critical to the final version of the paper.

626 **Open Research**

627 The data on which this article is based are available in Sweeney and Fu., 2023. Software required
628 to recreate the results is provided in Sweeney (2023).

629 **References**

- 630 Abalos, M., Randel, W. J., & Serrano, E. (2012). Variability in upwelling across the tropical
631 tropopause and correlations with tracers in the lower stratosphere. *Atmospheric Chemistry
632 and Physics*, 12(23), 11505–11517. <https://doi.org/10.5194/acp-12-11505-2012>
- 633 Abalos, Marta, Randel, W. J., & Serrano, E. (2014). Dynamical Forcing of Subseasonal
634 Variability in the Tropical Brewer–Dobson Circulation. *Journal of the Atmospheric
635 Sciences*, 71(9), 3439–3453. <https://doi.org/10.1175/JAS-D-13-0366.1>
- 636 Anthes, R. A., Bernhardt, P. A., Chen, Y., Cucurull, L., Dymond, K. F., Ector, D., et al. (2008).
637 The COSMIC/FORMOSAT-3 Mission: Early Results. *Bulletin of the American
638 Meteorological Society*, 89(3), 313–334. <https://doi.org/10.1175/BAMS-89-3-313>
- 639 Austin, J., & Reichler, T. J. (2008). Long-term evolution of the cold point tropical tropopause:
640 Simulation results and attribution analysis. *Journal of Geophysical Research: Atmospheres*,
641 113(D7). <https://doi.org/10.1029/2007JD009768>
- 642 Avery, M. A., Davis, S. M., Rosenlof, K. H., Ye, H., & Dessler, A. E. (2017). Large anomalies
643 in lower stratospheric water vapour and ice during the 2015–2016 El Niño. *Nature
644 Geoscience*, 10(6), 405–409. <https://doi.org/10.1038/ngeo2961>

- 645 Baldwin, M. P., Gray, L. J., Dunkerton, T. J., Hamilton, K., Haynes, P. H., Randel, W. J., et al.
646 (2001). The quasi-biennial oscillation. *Reviews of Geophysics*, 39(2), 179–229.
647 <https://doi.org/10.1029/1999RG000073>
- 648 Banerjee, A., Maycock, A. C., Archibald, A. T., Abraham, N. L., Telford, P., Braesicke, P., &
649 Pyle, J. A. (2016). Drivers of changes in stratospheric and tropospheric ozone between year
650 2000 and 2100. *Atmospheric Chemistry and Physics*, 16(5), 2727–2746.
651 <https://doi.org/10.5194/acp-16-2727-2016>
- 652 Birner, T., & Charlesworth, E. J. (2017). On the relative importance of radiative and dynamical
653 heating for tropical tropopause temperatures. *Journal of Geophysical Research:*
654 *Atmospheres*, 122(13), 6782–6797. <https://doi.org/10.1002/2016JD026445>
- 655 Boehm, M. T., & Lee, S. (2003). The Implications of Tropical Rossby Waves for Tropical
656 Tropopause Cirrus Formation and for the Equatorial Upwelling of the Brewer–Dobson
657 Circulation. *Journal of the Atmospheric Sciences*, 60(2), 247–261.
658 [https://doi.org/10.1175/1520-0469\(2003\)060<0247:TOTRW>2.0.CO;2](https://doi.org/10.1175/1520-0469(2003)060<0247:TOTRW>2.0.CO;2)
- 659 Boehm, M. T., & Verlinde, J. (2000). Stratospheric influence on upper tropospheric tropical
660 cirrus. *Geophysical Research Letters*, 27(19), 3209–3212.
661 <https://doi.org/10.1029/2000GL011678>
- 662 Bourguet, S., & Linz, M. (2023). Weakening of the tropical tropopause layer cold trap with
663 global warming. *Atmospheric Chemistry and Physics*, 23(13), 7447–7460.
664 <https://doi.org/10.5194/acp-23-7447-2023>
- 665 Bramberger, M., Alexander, M. J., Davis, S., Podglajen, A., Hertzog, A., Kalnajs, L., et al.
666 (2022). First Super-Pressure Balloon-Borne Fine-Vertical-Scale Profiles in the Upper TTL:

- 667 Impacts of Atmospheric Waves on Cirrus Clouds and the QBO. *Geophysical Research*
668 *Letters*, 49(5), e2021GL097596. <https://doi.org/10.1029/2021GL097596>
- 669 Brewer, A. W. (1949). Evidence for a world circulation provided by the measurements of helium
670 and water vapour distribution in the stratosphere. *Quarterly Journal of the Royal*
671 *Meteorological Society*, 75(326), 351–363. <https://doi.org/10.1002/qj.49707532603>
- 672 Butchart, N., Anstey, J. A., Kawatani, Y., Osprey, S. M., Richter, J. H., & Wu, T. (2020). QBO
673 Changes in CMIP6 Climate Projections. *Geophysical Research Letters*, 47(7),
674 e2019GL086903. <https://doi.org/10.1029/2019GL086903>
- 675 Calvo, N., Garcia, R. R., Randel, W. J., & Marsh, D. R. (2010). Dynamical Mechanism for the
676 Increase in Tropical Upwelling in the Lowermost Tropical Stratosphere during Warm
677 ENSO Events. *Journal of the Atmospheric Sciences*, 67(7), 2331–2340.
678 <https://doi.org/10.1175/2010JAS3433.1>
- 679 Chang, K.-W., & L'Ecuyer, T. (2020). Influence of gravity wave temperature anomalies and
680 their vertical gradients on cirrus clouds in the tropical tropopause layer – a satellite-based
681 view. *Atmospheric Chemistry and Physics*, 20(21), 12499–12514.
682 <https://doi.org/10.5194/acp-20-12499-2020>
- 683 Charlesworth, E. J., Birner, T., & Albers, J. R. (2019). Ozone Transport-Radiation Feedbacks in
684 the Tropical Tropopause Layer. *Geophysical Research Letters*, 46(23), 14195–14202.
685 <https://doi.org/10.1029/2019GL084679>
- 686 Chiodo, G., Polvani, L. M., Marsh, D. R., Stenke, A., Ball, W., Rozanov, E., et al. (2018). The
687 Response of the Ozone Layer to Quadrupled CO₂ Concentrations. *Journal of Climate*,
688 31(10), 3893–3907. <https://doi.org/10.1175/JCLI-D-17-0492.1>

- 689 Corti, T., Luo, B. P., Fu, Q., Vomel, H., & Peter, T. (2006). The impact of cirrus clouds on
690 tropical troposphere-to-stratosphere transport. *Atmos. Chem. Phys.*, 9.
- 691 Coy, L., Newman, P. A., Strahan, S., & Pawson, S. (2020). Seasonal Variation of the Quasi-
692 Biennial Oscillation Descent. *Journal of Geophysical Research: Atmospheres*, 125(18),
693 e2020JD033077. <https://doi.org/10.1029/2020JD033077>
- 694 Das, S. S., & Suneeth, K. V. (2020). Seasonal and interannual variations of water vapor in the
695 upper troposphere and lower stratosphere over the Asian Summer Monsoon region- in
696 perspective of the tropopause and ocean-atmosphere interactions. *Journal of Atmospheric
697 and Solar-Terrestrial Physics*, 201, 105244. <https://doi.org/10.1016/j.jastp.2020.105244>
- 698 Davis, S. M., Liang, C. K., & Rosenlof, K. H. (2013). Interannual variability of tropical
699 tropopause layer clouds. *Geophysical Research Letters*, 40(11), 2862–2866.
700 <https://doi.org/10.1002/grl.50512>
- 701 Deckert, R., & Dameris, M. (2008). Higher tropical SSTs strengthen the tropical upwelling via
702 deep convection. *Geophysical Research Letters*, 35(10).
703 <https://doi.org/10.1029/2008GL033719>
- 704 Dessler, A. E., Schoeberl, M. R., Wang, T., Davis, S. M., & Rosenlof, K. H. (2013).
705 Stratospheric water vapor feedback. *Proceedings of the National Academy of Sciences*,
706 110(45), 18087–18091. <https://doi.org/10.1073/pnas.1310344110>
- 707 Dessler, A. E., Schoeberl, M. R., Wang, T., Davis, S. M., Rosenlof, K. H., & Vernier, J.-P.
708 (2014). Variations of stratospheric water vapor over the past three decades. *Journal of
709 Geophysical Research: Atmospheres*, 119(22), 12,588-12,598.
710 <https://doi.org/10.1002/2014JD021712>

- 711 Diallo, M., Riese, M., Birner, T., Konopka, P., Müller, R., Hegglin, M. I., et al. (2018). Response
712 of stratospheric water vapor and ozone to the unusual timing of El Niño and the QBO
713 disruption in 2015–2016. *Atmospheric Chemistry and Physics*, 18(17), 13055–13073.
714 <https://doi.org/10.5194/acp-18-13055-2018>
- 715 Ding, Q., & Fu, Q. (2018). A warming tropical central Pacific dries the lower stratosphere.
716 *Climate Dynamics*, 50(7), 2813–2827. <https://doi.org/10.1007/s00382-017-3774-y>
- 717 Dinh, T. P., Durran, D. R., & Ackerman, T. P. (2010). Maintenance of tropical tropopause layer
718 cirrus. *Journal of Geophysical Research: Atmospheres*, 115(D2).
719 <https://doi.org/10.1029/2009JD012735>
- 720 Dunkerton, T. (1990). Annual variation of deseasonalized mean flow acceleration in the
721 equatorial lower stratosphere. https://doi.org/10.2151/JMSJ1965.68.4_499
- 722 Eguchi, N., & Kodera, K. (2010). Impacts of Stratospheric Sudden Warming Event on Tropical
723 Clouds and Moisture Fields in the TTL: A Case Study. *Sola*, 6, 137–140.
724 <https://doi.org/10.2151/sola.2010-035>
- 725 de F. Forster, P. M., & Shine, K. P. (1999). Stratospheric water vapour changes as a possible
726 contributor to observed stratospheric cooling. *Geophysical Research Letters*, 26(21), 3309–
727 3312. <https://doi.org/10.1029/1999GL010487>
- 728 Flury, T., Wu, D. L., & Read, W. G. (2012). Correlation among cirrus ice content, water vapor
729 and temperature in the TTL as observed by CALIPSO and Aura/MLS. *Atmospheric*
730 *Chemistry and Physics*, 12(2), 683–691. <https://doi.org/10.5194/acp-12-683-2012>
- 731 Flury, Thomas, wu, D., & Read, W. (2012). Variability of the Brewer-Dobson circulation's
732 meridional and vertical branch using Aura/MLS water vapor. *Atmospheric Chemistry &*
733 *Physics Discussions*, 12, 21291–21320. <https://doi.org/10.5194/acpd-12-21291-2012>

- 734 Fu, Q., Lin, P., Solomon, S., & Hartmann, D. L. (2015). Observational evidence of strengthening
735 of the Brewer-Dobson circulation since 1980. *Journal of Geophysical Research:*
736 *Atmospheres*, 120(19), 10,214-10,228. <https://doi.org/10.1002/2015JD023657>
- 737 Fu, Qiang. (2013). Bottom up in the tropics. *Nature Climate Change*, 3(11), 957–958.
738 <https://doi.org/10.1038/nclimate2039>
- 739 Fu, Qiang, Hu, Y., & Yang, Q. (2007). Identifying the top of the tropical tropopause layer from
740 vertical mass flux analysis and CALIPSO lidar cloud observations. *Geophysical Research*
741 *Letters*, 34(14). <https://doi.org/10.1029/2007GL030099>
- 742 Fu, Qiang, Smith, M., & Yang, Q. (2018). The Impact of Cloud Radiative Effects on the Tropical
743 Tropopause Layer Temperatures. *Atmosphere*, 9(10), 377.
744 <https://doi.org/10.3390/atmos9100377>
- 745 Fueglistaler, S., & Haynes, P. H. (2005). Control of interannual and longer-term variability of
746 stratospheric water vapor. *Journal of Geophysical Research: Atmospheres*, 110(D24).
747 <https://doi.org/10.1029/2005JD006019>
- 748 Fueglistaler, S., Dessler, A. E., Dunkerton, T. J., Folkins, I., Fu, Q., & Mote, P. W. (2009).
749 Tropical tropopause layer. *Reviews of Geophysics*, 47(1).
750 <https://doi.org/10.1029/2008RG000267>
- 751 Garcia, R. R., & Randel, W. J. (2008). Acceleration of the Brewer–Dobson Circulation due to
752 Increases in Greenhouse Gases. *Journal of the Atmospheric Sciences*, 65(8), 2731–2739.
753 <https://doi.org/10.1175/2008JAS2712.1>
- 754 Garfinkel, C. I., & Hartmann, D. L. (2008). Different ENSO teleconnections and their effects on
755 the stratospheric polar vortex. *Journal of Geophysical Research: Atmospheres*, 113(D18).
756 <https://doi.org/10.1029/2008JD009920>

- 757 Garfinkel, C. I., Waugh, D. W., Oman, L. D., Wang, L., & Hurwitz, M. M. (2013). Temperature
758 trends in the tropical upper troposphere and lower stratosphere: Connections with sea
759 surface temperatures and implications for water vapor and ozone. *Journal of Geophysical*
760 *Research: Atmospheres*, 118(17), 9658–9672. <https://doi.org/10.1002/jgrd.50772>
- 761 Garfinkel, Chaim I, Gordon, A., Oman, L. D., Li, F., Davis, S., & Pawson, S. (2018). Nonlinear
762 response of tropical lower stratospheric temperature and water vapor to ENSO. *Atmospheric*
763 *Chemistry and Physics*, 18(7), 4597–4615. <https://doi.org/10.5194/acp-18-4597-2018>
- 764 Garfinkel, Chaim I., Harari, O., Ziskin Ziv, S., Rao, J., Morgenstern, O., Zeng, G., et al. (2021).
765 Influence of the El Niño–Southern Oscillation on entry stratospheric water vapor in coupled
766 chemistry–ocean CCM1 and CMIP6 models. *Atmospheric Chemistry and Physics*, 21(5),
767 3725–3740. <https://doi.org/10.5194/acp-21-3725-2021>
- 768 Garny, H., Dameris, M., Randel, W., Bodeker, G. E., & Deckert, R. (2011). Dynamically Forced
769 Increase of Tropical Upwelling in the Lower Stratosphere. *Journal of the Atmospheric*
770 *Sciences*, 68(6), 1214–1233. <https://doi.org/10.1175/2011JAS3701.1>
- 771 Get^{TEL}man, A., & Forster, P. M. de F. (2002). A Climatology of the Tropical Tropopause Layer.
772 *Journal of the Meteorological Society of Japan. Ser. II*, 80(4B), 911–924.
773 <https://doi.org/10.2151/jmsj.80.911>
- 774 Gettelman, A., Birner, T., Eyring, V., Akiyoshi, H., Bekki, S., Brühl, C., et al. (2009). The
775 Tropical Tropopause Layer 1960–2100. *Atmospheric Chemistry and Physics*, 9(5), 1621–
776 1637. <https://doi.org/10.5194/acp-9-1621-2009>
- 777 Gettelman, A., Hegglin, M. I., Son, S.-W., Kim, J., Fujiwara, M., Birner, T., et al. (2010).
778 Multimodel assessment of the upper troposphere and lower stratosphere: Tropics and global

- 779 trends. *Journal of Geophysical Research: Atmospheres*, 115(D3).
780 <https://doi.org/10.1029/2009JD013638>
- 781 Gettelman, Andrew, Forster, P. M. de F., Fujiwara, M., Fu, Q., Vömel, H., Gohar, L. K., et al.
782 (2004). Radiation balance of the tropical tropopause layer. *Journal of Geophysical*
783 *Research: Atmospheres*, 109(D7). <https://doi.org/10.1029/2003JD004190>
- 784 Grise, K. M., & Thompson, D. W. J. (2013). On the Signatures of Equatorial and Extratropical
785 Wave Forcing in Tropical Tropopause Layer Temperatures. *Journal of the Atmospheric*
786 *Sciences*, 70(4), 1084–1102. <https://doi.org/10.1175/JAS-D-12-0163.1>
- 787 Hardiman, S. C., Boutle, I. A., Bushell, A. C., Butchart, N., Cullen, M. J. P., Field, P. R., et al.
788 (2015). Processes Controlling Tropical Tropopause Temperature and Stratospheric Water
789 Vapor in Climate Models. *Journal of Climate*, 28(16), 6516–6535.
790 <https://doi.org/10.1175/JCLI-D-15-0075.1>
- 791 Haynes, P. H., McIntyre, M. E., Shepherd, T. G., Marks, C. J., & Shine, K. P. (1991). On the
792 “Downward Control” of Extratropical Diabatic Circulations by Eddy-Induced Mean Zonal
793 Forces. *Journal of the Atmospheric Sciences*, 48(4), 651–678. [https://doi.org/10.1175/1520-0469\(1991\)048<0651:OTCOED>2.0.CO;2](https://doi.org/10.1175/1520-0469(1991)048<0651:OTCOED>2.0.CO;2)
- 794 [https://doi.org/10.1175/1520-0469\(1991\)048<0651:OTCOED>2.0.CO;2](https://doi.org/10.1175/1520-0469(1991)048<0651:OTCOED>2.0.CO;2)
- 795 Hersbach, H., Bell, B., Berrisford, P., Hirahara, S., Horányi, A., Muñoz-Sabater, J., et al. (2020).
796 The ERA5 global reanalysis. *Quarterly Journal of the Royal Meteorological Society*,
797 146(730), 1999–2049. <https://doi.org/10.1002/qj.3803>
- 798 Holton, J., & Gettelman, A. (2001). Horizontal transport and dehydration in the stratosphere.
799 *Geophys. Res. Lett.*, 28, 2799–2802. <https://doi.org/10.1029/2001GL013148>

- 800 Holton, J., Haynes, P., McIntyre, M., Douglass, A., Rood, R., & Pfister, L. (1995). Stratosphere-
801 Troposphere Exchange. *Reviews of Geophysics - REV GEOPHYS*, 33.
802 <https://doi.org/10.1029/95RG02097>
- 803 Jensen, E. J., Toon, O. B., Pfister, L., & Selkirk, H. B. (1996). Dehydration of the upper
804 troposphere and lower stratosphere by subvisible cirrus clouds near the tropical tropopause.
805 *Geophysical Research Letters*, 23(8), 825–828. <https://doi.org/10.1029/96GL00722>
- 806 Jensen, E. J., Diskin, G., Lawson, R. P., Lance, S., Bui, T. P., Hlavka, D., et al. (2013). Ice
807 nucleation and dehydration in the Tropical Tropopause Layer. *Proceedings of the National*
808 *Academy of Sciences*, 110(6), 2041–2046. <https://doi.org/10.1073/pnas.1217104110>
- 809 Joshi, M. M., Webb, M. J., Maycock, A. C., & Collins, M. (2010). Stratospheric water vapour
810 and high climate sensitivity in a version of the HadSM3 climate model. *Atmospheric*
811 *Chemistry and Physics*, 10(15), 7161–7167. <https://doi.org/10.5194/acp-10-7161-2010>
- 812 Kim, J., Randel, W. J., Birner, T., & Abalos, M. (2016). Spectrum of Wave Forcing Associated
813 with the Annual Cycle of Upwelling at the Tropical Tropopause. *Journal of the*
814 *Atmospheric Sciences*, 73(2), 855–868. <https://doi.org/10.1175/JAS-D-15-0096.1>
- 815 Kim, J.-E., & Alexander, M. J. (2015). Direct impacts of waves on tropical cold point tropopause
816 temperature. *Geophysical Research Letters*, 42(5), 1584–1592.
817 <https://doi.org/10.1002/2014GL062737>
- 818 Kim, J.-E., Alexander, M. J., Bui, T. P., Dean-Day, J. M., Lawson, R. P., Woods, S., et al.
819 (2016). Ubiquitous influence of waves on tropical high cirrus clouds. *Geophysical Research*
820 *Letters*, 43(11), 5895–5901. <https://doi.org/10.1002/2016GL069293>

- 821 Kirk-Davidoff, D. B., Hints, E. J., Anderson, J. G., & Keith, D. W. (1999). The effect of climate
822 change on ozone depletion through changes in stratospheric water vapour. *Nature*,
823 *402*(6760), 399–401. <https://doi.org/10.1038/46521>
- 824 Konopka, P., Grooß, J.-U., Plöger, F., & Müller, R. (2009). Annual cycle of horizontal in-mixing
825 into the lower tropical stratosphere. *Journal of Geophysical Research: Atmospheres*,
826 *114*(D19). <https://doi.org/10.1029/2009JD011955>
- 827 Konopka, P., Ploeger, F., Tao, M., & Riese, M. (2016). Zonally resolved impact of ENSO on the
828 stratospheric circulation and water vapor entry values. *Journal of Geophysical Research:*
829 *Atmospheres*, *121*(19), 11,486–11,501. <https://doi.org/10.1002/2015JD024698>
- 830 Kuo, Y.-H., Wee, T.-K., Sokolovskiy, S., Rocken, C., Schreiner, W., Hunt, D., & Anthes, R. A.
831 (2004). Inversion and Error Estimation of GPS Radio Occultation Data. *Journal of the*
832 *Meteorological Society of Japan. Ser. II*, *82*(1B), 507–531.
833 <https://doi.org/10.2151/jmsj.2004.507>
- 834 Kursinski, E. R., Hajj, G. A., Schofield, J. T., Linfield, R. P., & Hardy, K. R. (1997). Observing
835 Earth’s atmosphere with radio occultation measurements using the Global Positioning
836 System. *Journal of Geophysical Research: Atmospheres*, *102*(D19), 23429–23465.
837 <https://doi.org/10.1029/97JD01569>
- 838 Li, Y., & Thompson, D. W. J. (2013). The signature of the stratospheric Brewer–Dobson
839 circulation in tropospheric clouds. *Journal of Geophysical Research: Atmospheres*, *118*(9),
840 3486–3494. <https://doi.org/10.1002/jgrd.50339>
- 841 Liang, C. K., Eldering, A., Gettelman, A., Tian, B., Wong, S., Fetzer, E. J., & Liou, K. N.
842 (2011). Record of tropical interannual variability of temperature and water vapor from a

- 843 combined AIRS-MLS data set. *Journal of Geophysical Research: Atmospheres*, 116(D6).
844 <https://doi.org/10.1029/2010JD014841>
- 845 Lin, P., & Fu, Q. (2013). Changes in various branches of the Brewer–Dobson circulation from an
846 ensemble of chemistry climate models. *Journal of Geophysical Research: Atmospheres*,
847 118(1), 73–84. <https://doi.org/10.1029/2012JD018813>
- 848 Lin, Pu, Fu, Q., Solomon, S., & Wallace, J. M. (2009). Temperature Trend Patterns in Southern
849 Hemisphere High Latitudes: Novel Indicators of Stratospheric Change. *Journal of Climate*,
850 22(23), 6325–6341. <https://doi.org/10.1175/2009JCLI2971.1>
- 851 Lin, Pu, Paynter, D., Ming, Y., & Ramaswamy, V. (2017). Changes of the Tropical Tropopause
852 Layer under Global Warming. *Journal of Climate*, 30(4), 1245–1258.
853 <https://doi.org/10.1175/JCLI-D-16-0457.1>
- 854 Lindeman, R. H., Merenda, P. F., & Gold, R. Z. (1980). *Introduction to bivariate and*
855 *multivariate analysis*. Glenview, Ill: Scott, Foresman.
- 856 Livesey, N. J., Read, W. G., Froidevaux, L., Lambert, A., Santee, M. L., Schwartz, M. J., et al.
857 (2021). Investigation and amelioration of long-term instrumental drifts in water vapor and
858 nitrous oxide measurements from the Aura Microwave Limb Sounder (MLS) and their
859 implications for studies of variability and trends. *Atmospheric Chemistry and Physics*,
860 21(20), 15409–15430. <https://doi.org/10.5194/acp-21-15409-2021>
- 861 Lorenz, D. J., & DeWeaver, E. T. (2007). Tropopause height and zonal wind response to global
862 warming in the IPCC scenario integrations. *Journal of Geophysical Research: Atmospheres*,
863 112(D10). <https://doi.org/10.1029/2006JD008087>

- 864 Lu, J., Xie, F., Sun, C., Luo, J., Cai, Q., Zhang, J., et al. (2020). Analysis of factors influencing
865 tropical lower stratospheric water vapor during 1980–2017. *Npj Climate and Atmospheric*
866 *Science*, 3(1), 1–11. <https://doi.org/10.1038/s41612-020-00138-7>
- 867 Madden, R. A., & Julian, P. R. (1971). Detection of a 40–50 Day Oscillation in the Zonal Wind
868 in the Tropical Pacific. *Journal of the Atmospheric Sciences*, 28(5), 702–708.
869 [https://doi.org/10.1175/1520-0469\(1971\)028<0702:DOADOI>2.0.CO;2](https://doi.org/10.1175/1520-0469(1971)028<0702:DOADOI>2.0.CO;2)
- 870 Marsh, D. R., & Garcia, R. R. (2007). Attribution of decadal variability in lower-stratospheric
871 tropical ozone. *Geophysical Research Letters*, 34(21).
872 <https://doi.org/10.1029/2007GL030935>
- 873 Martin, Z., Sobel, A., Butler, A., & Wang, S. (2021). Variability in QBO Temperature
874 Anomalies on Annual and Decadal Time Scales. *Journal of Climate*, 34(2), 589–605.
875 <https://doi.org/10.1175/JCLI-D-20-0287.1>
- 876 Match, A., & Gerber, E. P. (2022). Tropospheric Expansion Under Global Warming Reduces
877 Tropical Lower Stratospheric Ozone. *Geophysical Research Letters*, 49(19),
878 e2022GL099463. <https://doi.org/10.1029/2022GL099463>
- 879 McFarquhar, G. M., Heymsfield, A. J., Spinhirne, J., & Hart, B. (2000). Thin and Subvisual
880 Tropopause Tropical Cirrus: Observations and Radiative Impacts. *Journal of the*
881 *Atmospheric Sciences*, 57(12), 1841–1853. [https://doi.org/10.1175/1520-0469\(2000\)057<1841:TASTTC>2.0.CO;2](https://doi.org/10.1175/1520-0469(2000)057<1841:TASTTC>2.0.CO;2)
- 882
- 883 Mote, P. W., Rosenlof, K. H., McIntyre, M. E., Carr, E. S., Gille, J. C., Holton, J. R., et al.
884 (1996). An atmospheric tape recorder: The imprint of tropical tropopause temperatures on
885 stratospheric water vapor. *Journal of Geophysical Research: Atmospheres*, 101(D2), 3989–
886 4006. <https://doi.org/10.1029/95JD03422>

- 887 Oman, L., Waugh, D. W., Pawson, S., Stolarski, R. S., & Nielsen, J. E. (2008). Understanding
888 the Changes of Stratospheric Water Vapor in Coupled Chemistry–Climate Model
889 Simulations. *Journal of the Atmospheric Sciences*, 65(10), 3278–3291.
890 <https://doi.org/10.1175/2008JAS2696.1>
- 891 Ortland, D. A., & Alexander, M. J. (2014). The Residual-Mean Circulation in the Tropical
892 Tropopause Layer Driven by Tropical Waves. *Journal of the Atmospheric Sciences*, 71(4),
893 1305–1322. <https://doi.org/10.1175/JAS-D-13-0100.1>
- 894 Pahlavan, H. A., Fu, Q., Wallace, J. M., & Kiladis, G. N. (2021). Revisiting the Quasi-Biennial
895 Oscillation as Seen in ERA5. Part I: Description and Momentum Budget. *Journal of the*
896 *Atmospheric Sciences*, 78(3), 673–691. <https://doi.org/10.1175/JAS-D-20-0248.1>
- 897 Philander, G. (1990). Geophysical Interplays: *El Niño, La Niña, and the Southern Oscillation*. S.
898 George Philander. Academic Press, San Diego, CA, 1989. x, 293 pp., illus. \$59.50.
899 International Geophysics Series, vol. 46. *Science*, 248(4957), 904–905.
900 <https://doi.org/10.1126/science.248.4957.904>
- 901 Plumb, R. A., & Bell, R. C. (1982). Equatorial waves in steady zonal shear flow. *Quarterly*
902 *Journal of the Royal Meteorological Society*, 108(456), 313–334.
903 <https://doi.org/10.1002/qj.49710845603>
- 904 Plumb, R. A., & Eluszkiewicz, J. (1999). The Brewer–Dobson Circulation: Dynamics of the
905 Tropical Upwelling. *Journal of the Atmospheric Sciences*, 56(6), 868–890.
906 [https://doi.org/10.1175/1520-0469\(1999\)056<0868:TBDCDO>2.0.CO;2](https://doi.org/10.1175/1520-0469(1999)056<0868:TBDCDO>2.0.CO;2)
- 907 Podglajen, A., Hertzog, A., Plougonven, R., & Legras, B. (2016). Lagrangian temperature and
908 vertical velocity fluctuations due to gravity waves in the lower stratosphere. *Geophysical*
909 *Research Letters*, 43(7), 3543–3553. <https://doi.org/10.1002/2016GL068148>

- 910 Podglajen, A., Plougonven, R., Hertzog, A., & Jensen, E. (2018). Impact of gravity waves on the
911 motion and distribution of atmospheric ice particles. *Atmospheric Chemistry and Physics*,
912 *18*(14), 10799–10823. <https://doi.org/10.5194/acp-18-10799-2018>
- 913 Randel, W., & Park, M. (2019). Diagnosing Observed Stratospheric Water Vapor Relationships
914 to the Cold Point Tropical Tropopause. *Journal of Geophysical Research: Atmospheres*,
915 *124*(13), 7018–7033. <https://doi.org/10.1029/2019JD030648>
- 916 Randel, W. J., & Jensen, E. J. (2013). Physical processes in the tropical tropopause layer and
917 their roles in a changing climate. *Nature Geoscience*, *6*(3), 169–176.
918 <https://doi.org/10.1038/ngeo1733>
- 919 Randel, W. J., & Wu, F. (2015). Variability of Zonal Mean Tropical Temperatures Derived from
920 a Decade of GPS Radio Occultation Data. *Journal of the Atmospheric Sciences*, *72*(3),
921 1261–1275. <https://doi.org/10.1175/JAS-D-14-0216.1>
- 922 Randel, W. J., Wu, F., & Gaffen, D. J. (2000). Interannual variability of the tropical tropopause
923 derived from radiosonde data and NCEP reanalyses. *Journal of Geophysical Research:*
924 *Atmospheres*, *105*(D12), 15509–15523. <https://doi.org/10.1029/2000JD900155>
- 925 Randel, W. J., Garcia, R. R., & Wu, F. (2002). Time-Dependent Upwelling in the Tropical
926 Lower Stratosphere Estimated from the Zonal-Mean Momentum Budget. *Journal of the*
927 *Atmospheric Sciences*, *59*(13), 2141–2152. [https://doi.org/10.1175/1520-0469\(2002\)059<2141:TDUITT>2.0.CO;2](https://doi.org/10.1175/1520-0469(2002)059<2141:TDUITT>2.0.CO;2)
- 928
929 Randel, W. J., Park, M., Wu, F., & Livesey, N. (2007). A Large Annual Cycle in Ozone above
930 the Tropical Tropopause Linked to the Brewer–Dobson Circulation. *Journal of the*
931 *Atmospheric Sciences*, *64*(12), 4479–4488. <https://doi.org/10.1175/2007JAS2409.1>

- 932 Randel, W. J., Garcia, R., & Wu, F. (2008). Dynamical Balances and Tropical Stratospheric
933 Upwelling. *Journal of the Atmospheric Sciences*, 65(11), 3584–3595.
934 <https://doi.org/10.1175/2008JAS2756.1>
- 935 Randel, W. J., Garcia, R. R., Calvo, N., & Marsh, D. (2009). ENSO influence on zonal mean
936 temperature and ozone in the tropical lower stratosphere. *Geophysical Research Letters*,
937 36(15). <https://doi.org/10.1029/2009GL039343>
- 938 Randel, W. J., Park, M., Emmons, L., Kinnison, D., Bernath, P., Walker, K. A., et al. (2010).
939 Asian Monsoon Transport of Pollution to the Stratosphere. *Science*, 328(5978), 611–613.
940 <https://doi.org/10.1126/science.1182274>
- 941 Read, W. G., Lambert, A., Bacmeister, J., Cofield, R. E., Christensen, L. E., Cuddy, D. T., et al.
942 (2007). Aura Microwave Limb Sounder upper tropospheric and lower stratospheric H₂O
943 and relative humidity with respect to ice validation. *Journal of Geophysical Research*
944 (*Atmospheres*), 112, D24S35. <https://doi.org/10.1029/2007JD008752>
- 945 Richter, J. H., Anstey, J. A., Butchart, N., Kawatani, Y., Meehl, G. A., Osprey, S., & Simpson, I.
946 R. (2020). Progress in Simulating the Quasi-Biennial Oscillation in CMIP Models. *Journal*
947 *of Geophysical Research: Atmospheres*, 125(8), e2019JD032362.
948 <https://doi.org/10.1029/2019JD032362>
- 949 Rosenlof, K. H. (1995). Seasonal cycle of the residual mean meridional circulation in the
950 stratosphere. *Journal of Geophysical Research*, 100, 5173–5191.
951 <https://doi.org/10.1029/94JD03122>
- 952 Santee, M. L., Manney, G. L., Livesey, N. J., Schwartz, M. J., Neu, J. L., & Read, W. G. (2017).
953 A comprehensive overview of the climatological composition of the Asian summer
954 monsoon anticyclone based on 10 years of Aura Microwave Limb Sounder measurements.

- 955 *Journal of Geophysical Research: Atmospheres*, 122(10), 5491–5514.
- 956 <https://doi.org/10.1002/2016JD026408>
- 957 Santer, B. D., Sausen, R., Wigley, T. M. L., Boyle, J. S., AchutaRao, K., Doutriaux, C., et al.
- 958 (2003). Behavior of tropopause height and atmospheric temperature in models, reanalyses,
- 959 and observations: Decadal changes. *Journal of Geophysical Research: Atmospheres*,
- 960 108(D1), ACL 1-1-ACL 1-22. <https://doi.org/10.1029/2002JD002258>
- 961 Scherllin-Pirscher, B., Deser, C., Ho, S.-P., Chou, C., Randel, W., & Kuo, Y.-H. (2012). The
- 962 vertical and spatial structure of ENSO in the upper troposphere and lower stratosphere from
- 963 GPS radio occultation measurements. *Geophysical Research Letters*, 39(20).
- 964 <https://doi.org/10.1029/2012GL053071>
- 965 Schreiner, W. s., Weiss, J. p., Anthes, R. a., Braun, J., Chu, V., Fong, J., et al. (2020). COSMIC-
- 966 2 Radio Occultation Constellation: First Results. *Geophysical Research Letters*, 47(4),
- 967 e2019GL086841. <https://doi.org/10.1029/2019GL086841>
- 968 Shepherd, T. G., & McLandress, C. (2011). A Robust Mechanism for Strengthening of the
- 969 Brewer–Dobson Circulation in Response to Climate Change: Critical-Layer Control of
- 970 Subtropical Wave Breaking. *Journal of the Atmospheric Sciences*, 68(4), 784–797.
- 971 <https://doi.org/10.1175/2010JAS3608.1>
- 972 Sokol, A. B., & Hartmann, D. L. (2020). Tropical Anvil Clouds: Radiative Driving Toward a
- 973 Preferred State. *Journal of Geophysical Research: Atmospheres*, 125(21), e2020JD033107.
- 974 <https://doi.org/10.1029/2020JD033107>
- 975 Solomon, S., Rosenlof, K. H., Portmann, R. W., Daniel, J. S., Davis, S. M., Sanford, T. J., &
- 976 Plattner, G.-K. (2010). Contributions of Stratospheric Water Vapor to Decadal Changes in

- 977 the Rate of Global Warming. *Science*, 327(5970), 1219–1223.
978 <https://doi.org/10.1126/science.1182488>
- 979 Solomon, S., Ivy, D. J., Kinnison, D., Mills, M. J., Neely, R. R., & Schmidt, A. (2016).
980 Emergence of healing in the Antarctic ozone layer. *Science*, 353(6296), 269–274.
981 <https://doi.org/10.1126/science.aae0061>
- 982 Sunilkumar, S. V., Parameswaran, K., Rajeev, K., Krishna Murthy, B. V., Meenu, S., Mehta, S.
983 K., & Babu, A. (2010). Semitransparent cirrus clouds in the tropical tropopause layer during
984 two contrasting seasons. *Journal of Atmospheric and Solar-Terrestrial Physics*, 72(9), 745–
985 762. <https://doi.org/10.1016/j.jastp.2010.03.020>
- 986 Sweeney, A., Fu, Q., Interannual Variability of Zonal Mean Temperature, Water Vapor, and
987 Clouds in the Tropical Tropopause Layer [Data set]. Zenodo.
988 <https://zenodo.org/records/10045808>
- 989 Sweeney A., (2023). October 18, 2023 Release Version (1.0.0) AodhanSweeney/TTLVariability
990 [Software]. GitHub. <https://github.com/AodhanSweeney/TTLVariability>
- 991 Sweeney, A., Fu, Q., Pahlavan, H. A., & Haynes, P. (2023). Seasonality of the QBO Impact on
992 Equatorial Clouds. *Journal of Geophysical Research: Atmospheres*, 128(7),
993 e2022JD037737. <https://doi.org/10.1029/2022JD037737>
- 994 Sweeney, A. J., & Fu, Q. (2021). Diurnal Cycles of Synthetic Microwave Sounding Lower-
995 Stratospheric Temperatures from Radio Occultation Observations, Reanalysis, and Model
996 Simulations. *Journal of Atmospheric and Oceanic Technology*, 38(12), 2045–2059.
997 <https://doi.org/10.1175/JTECH-D-21-0071.1>
- 998 Tegtmeier, S., Anstey, J., Davis, S., Ivanciu, I., Jia, Y., McPhee, D., & Pilch Kedzierski, R.
999 (2020). Zonal Asymmetry of the QBO Temperature Signal in the Tropical Tropopause

- 1000 Region. *Geophysical Research Letters*, 47(24), e2020GL089533.
- 1001 <https://doi.org/10.1029/2020GL089533>
- 1002 Thornberry, T. D., Rollins, A. W., Avery, M. A., Woods, S., Lawson, R. P., Bui, T. V., & Gao,
1003 R.-S. (2017). Ice water content-extinction relationships and effective diameter for TTL
1004 cirrus derived from in situ measurements during ATTREX 2014. *Journal of Geophysical*
1005 *Research: Atmospheres*, 122(8), 4494–4507. <https://doi.org/10.1002/2016JD025948>
- 1006 Thorsen, T. J., Fu, Q., Comstock, J. M., Sivaraman, C., Vaughan, M. A., Winker, D. M., &
1007 Turner, D. D. (2013). Macrophysical properties of tropical cirrus clouds from the CALIPSO
1008 satellite and from ground-based micropulse and Raman lidars. *Journal of Geophysical*
1009 *Research: Atmospheres*, 118(16), 9209–9220. <https://doi.org/10.1002/jgrd.50691>
- 1010 Tian, E. W., Su, H., Tian, B., & Jiang, J. H. (2019). Interannual variations of water vapor in the
1011 tropical upper troposphere and the lower and middle stratosphere and their connections to
1012 ENSO and QBO. *Atmospheric Chemistry and Physics*, 19(15), 9913–9926.
1013 <https://doi.org/10.5194/acp-19-9913-2019>
- 1014 Tseng, H. -H., & Fu, Q. (2017). Tropical tropopause layer cirrus and its relation to tropopause.
1015 *Journal of Quantitative Spectroscopy and Radiative Transfer*, 188, 118–131.
1016 <https://doi.org/10.1016/j.jqsrt.2016.05.029>
- 1017 Tseng, Hsiu-Hui, & Fu, Q. (2017). Temperature Control of the Variability of Tropical
1018 Tropopause Layer Cirrus Clouds. *Journal of Geophysical Research: Atmospheres*, 122(20),
1019 11,062-11,075. <https://doi.org/10.1002/2017JD027093>
- 1020 Tweedy, O. V., Waugh, D. W., Randel, W. J., Abalos, M., Oman, L. D., & Kinnison, D. E.
1021 (2018). The Impact of Boreal Summer ENSO Events on Tropical Lower Stratospheric

- 1022 Ozone. *Journal of Geophysical Research: Atmospheres*, 123(17), 9843–9857.
1023 <https://doi.org/10.1029/2018JD029020>
- 1024 Ueyama, R., Jensen, E. J., Pfister, L., & Kim, J.-E. (2015). Dynamical, convective, and
1025 microphysical control on wintertime distributions of water vapor and clouds in the tropical
1026 tropopause layer. *Journal of Geophysical Research: Atmospheres*, 120(19), 10,483-10,500.
1027 <https://doi.org/10.1002/2015JD023318>
- 1028 Ueyama, R., Jensen, E. J., & Pfister, L. (2018). Convective Influence on the Humidity and
1029 Clouds in the Tropical Tropopause Layer During Boreal Summer. *Journal of Geophysical
1030 Research: Atmospheres*, 123(14), 7576–7593. <https://doi.org/10.1029/2018JD028674>
- 1031 Ventrice, M., Wheeler, M., Hendon, H., Iii, S., Thorncroft, C., & Kiladis, G. (2013). A Modified
1032 Multivariate Madden-Julian Oscillation Index Using Velocity Potential. *Monthly Weather
1033 Review*, 141, 4197–4210. <https://doi.org/10.1175/MWR-D-12-00327.1>
- 1034 Virts, K. S., & Wallace, J. M. (2014). Observations of Temperature, Wind, Cirrus, and Trace
1035 Gases in the Tropical Tropopause Transition Layer during the MJO. *Journal of the
1036 Atmospheric Sciences*, 71(3), 1143–1157. <https://doi.org/10.1175/JAS-D-13-0178.1>
- 1037 Virts, K. S., Wallace, J. M., Fu, Q., & Ackerman, T. P. (2010). Tropical Tropopause Transition
1038 Layer Cirrus as Represented by CALIPSO Lidar Observations. *Journal of the Atmospheric
1039 Sciences*, 67(10), 3113–3129. <https://doi.org/10.1175/2010JAS3412.1>
- 1040 Walker, J. M., Bordoni, S., & Schneider, T. (2015). Interannual Variability in the Large-Scale
1041 Dynamics of the South Asian Summer Monsoon. *Journal of Climate*, 28(9), 3731–3750.
1042 <https://doi.org/10.1175/JCLI-D-14-00612.1>

- 1043 Wang, M., & Fu, Q. (2021). Stratosphere-Troposphere Exchange of Air Masses and Ozone
1044 Concentrations Based on Reanalyses and Observations. *Journal of Geophysical Research:*
1045 *Atmospheres*, 126(18), e2021JD035159. <https://doi.org/10.1029/2021JD035159>
- 1046 Wang, M., & Fu, Q. (2023). Changes in Stratosphere-Troposphere Exchange of Air Mass and
1047 Ozone Concentration in CCMI Models From 1960 to 2099. *Journal of Geophysical*
1048 *Research: Atmospheres*, 128(13), e2023JD038487. <https://doi.org/10.1029/2023JD038487>
- 1049 Wang, T., Wu, D. L., Gong, J., & Tsai, V. (2019). Tropopause Laminae and Its Role in the
1050 Lower Stratosphere Total Water Budget. *Journal of Geophysical Research: Atmospheres*,
1051 124(13), 7034–7052. <https://doi.org/10.1029/2018JD029845>
- 1052 Winker, D. M., Pelon, J., Coakley, J. A., Ackerman, S. A., Charlson, R. J., Colarco, P. R., et al.
1053 (2010). The CALIPSO Mission: A Global 3D View of Aerosols and Clouds. *Bulletin of the*
1054 *American Meteorological Society*, 91(9), 1211–1230.
1055 <https://doi.org/10.1175/2010BAMS3009.1>
- 1056 Wu, Y., & Zheng, C. (2022). Summertime Transport Pathways and Dynamics From Northern
1057 India and Tibetan Plateau to the Lower Stratosphere: Insights From Idealized Tracer
1058 Experiments. *Journal of Geophysical Research: Atmospheres*, 127(9), e2021JD036399.
1059 <https://doi.org/10.1029/2021JD036399>
- 1060 Xie, F., Li, J., Tian, W., Li, Y., & Feng, J. (2014). Indo-Pacific Warm Pool Area Expansion,
1061 Modoki Activity and Tropical Cold-Point Tropopause Temperature Variations. *Scientific*
1062 *Reports*, 4(1), 4552. <https://doi.org/10.1038/srep04552>
- 1063 Yang, Q., Fu, Q., & Hu, Y. (2010). Radiative impacts of clouds in the tropical tropopause layer.
1064 *Journal of Geophysical Research: Atmospheres*, 115(D4).
1065 <https://doi.org/10.1029/2009JD012393>

- 1066 Ye, H., Dessler, A. E., & Yu, W. (2018). Effects of convective ice evaporation on interannual
1067 variability of tropical tropopause layer water vapor. *Atmospheric Chemistry and Physics*,
1068 *18*(7), 4425–4437. <https://doi.org/10.5194/acp-18-4425-2018>
- 1069 Yoo, C., & Son, S.-W. (2016). Modulation of the boreal wintertime Madden-Julian oscillation by
1070 the stratospheric quasi-biennial oscillation. *Geophysical Research Letters*, *43*(3), 1392–
1071 1398. <https://doi.org/10.1002/2016GL067762>
- 1072 Yulaeva, E., Holton, J. R., & Wallace, J. M. (1994). On the Cause of the Annual Cycle in
1073 Tropical Lower-Stratospheric Temperatures. *Journal of the Atmospheric Sciences*, *51*(2),
1074 169–174. [https://doi.org/10.1175/1520-0469\(1994\)051<0169:OTCOTA>2.0.CO;2](https://doi.org/10.1175/1520-0469(1994)051<0169:OTCOTA>2.0.CO;2)
- 1075 Zeng, Z., Sokolovskiy, S., Schreiner, W. S., & Hunt, D. (2019). Representation of Vertical
1076 Atmospheric Structures by Radio Occultation Observations in the Upper Troposphere and
1077 Lower Stratosphere: Comparison to High-Resolution Radiosonde Profiles. *Journal of*
1078 *Atmospheric and Oceanic Technology*, *36*(4), 655–670. [https://doi.org/10.1175/JTECH-D-](https://doi.org/10.1175/JTECH-D-18-0105.1)
1079 [18-0105.1](https://doi.org/10.1175/JTECH-D-18-0105.1)
- 1080 Zhou, C., Dessler, A. E., Zelinka, M. D., Yang, P., & Wang, T. (2014). Cirrus feedback on
1081 interannual climate fluctuations. *Geophysical Research Letters*, *41*(24), 9166–9173.
1082 <https://doi.org/10.1002/2014GL062095>
- 1083 Ziskin Ziv, S., Garfinkel, C. I., Davis, S., & Banerjee, A. (2022). The roles of the Quasi-Biennial
1084 Oscillation and El Niño for entry stratospheric water vapor in observations and coupled
1085 chemistry–ocean CCM1 and CMIP6 models. *Atmospheric Chemistry and Physics*, *22*(11),
1086 7523–7538. <https://doi.org/10.5194/acp-22-7523-2022>
- 1087